Functional Analysis of Ostm1 gene in neuronal physiology

Hye In Kim (Hailey)

Master of Science

Faculty of Graduate Studies

McGill University

Montreal, Quebec, Canada

December 2014

A thesis submitted to McGill University in partial fulfillement of the requirements of the degree of Master of Science

DEDICATION

I dedicate this thesis to God for his love and faithfulness.

I also want to thank my loving family. Special thanks to my father, Sucbong Kim, who has always trusted in me and supported every decision I made. To my mother in heaven, Kyunghyoun Lee, for always being there for me. To my lovely little sisters, Hyewon Kim and Hyemin Kim, for caring and understanding.

ACKNOWLEDGMENTS

I would like to acknowledge and thank my supervisor, Dr. Jean Vacher. It was an honorable experience for me to be in such a wonderful lab. Dr. Vacher provided me with support and patience even as I was struggling. I thank Dr. Vacher for his challenging discussions and guidance as well as for financial support, allowing me to focus on my research and degree.

My next acknowledgement goes to the members of the lab: Dr. Subramanya N. M. Pandruvada for giving me advices and training me in neuronal culture and Immunohistochemistry; Marie Mutabaruka for all the conversations, advices and support throughout the whole program; Monica Pata for simply being a wonderful person. Her caring is truly appreciated. I am very grateful to have all the excellent colleagues during my stay at the Vacher lab.

I also would like to acknowledge Dr. Joseph Rochford and his team in Douglas institute research center for performing the behavior test and engaging in kind discussions.

TABLE OF CONTENTS

LIST OF TABLES

LIST OF FIGURES

ABBREVIATIONS

ADO: Autosomal Dominant Osteopetrosis

Akt: protein kinase B

ARO: Autosomal Recessive Osteopetrosis

Atg: Autophagy related protein

BAC: Bacterial Artificial Chromosome

BMD: Bone Marrow Density

CA3: Cornu Ammonis 3

CAII: Carbonic Anhydrase

ClC-7: Cl- - H+ exchange transporter 7

CNS: Central Nervous System

DG: Dentate gyrus

DRG: Dorsal Root Ganglion

ES: Embryonic Stem

FACS: Fluorescence-Activated Cell Sorting

GFAP: Glial Fibrillary Acidic Protein

gl: grey-lethal

H&E: Hematoxylin and Eosin

HD: Huntington's Disease

HRP: Horseradish Peroxidase

HSCT: Hematopoietic Stem Cell Transplantation

IGF: Insulin-like Growth Factor 1

IRO: Intermediate autosomal Recessive Osteopetrosis

ITI: Inter-Trial Interval

LC3: microtubule-associated protein 1 Light Chain 3

MAPK: Mitogen-Activated Protein Kinases

M-CSF: Macrophage Colony Stimulating Factor

MITF: Microphthalamia-Associated Transcription Factor

MRI: Magnetic Resonance Imaging

mTOR: mammalian Target Of Rapamycin

NFkB: Nuclear Factor kappa-light-chain-enhancer of activated B cells

ORF: Open Reading Frame

Ostm1: Osteopetrosis Associated Transmembrane Protein 1

Pax1: Paied box 1

PCR: Polymerase Chain Reaction

PI-3K: Phosphatidylinositol-4,5-bisphosphate 3-Kinase

PX: Phox homology

qPCR: Real-time Polymerase Chain Reaction

RANK: Receptor Activator of Nuclear factor Kappa-B

RANKL: Receptor Activator of Nuclear factor Kappa-B Ligand

RPM: Revolutions Per Minute

RT-PCR: Reverse Transcription Polymerase Chain Reaction

SNX10: Sorting Nexin 10

SYN: Synapsin

TRAP: Tartrate-Resistant Acid Phosphatase

V-ATPase: ATP-dependent osteoclast-specific Vacuolar proton pump

WT: wild-type

ABSTRACT

Autosomal recessive malignant osteopetrosis (ARO) is an inherited bone disorder resulting from defective hematopoietic lineage derived osteoclasts. We have previously characterized an *Ostm1* gene that is responsible for the spontaneous murine osteopetrotic grey-lethal phenotype and obtained functional rescue of hematopoietic defects in PU.1-*Ostm1-gl/gl* mice. However, previous analysis of the PU.1-*Ostm1-gl/gl* mice suggested a primary role of Ostm1 in neuronal cells; this was further supported by the characterization of brain anomalies in human *OSTM1*-related ARO patients. In order to investigate the function of Ostm1 in neuronal cells, neuron specific conditional knockout mice were generated following genetic ablation with SYN1-Cre deleter mice. The *Ostm1*$^{lox/lox}$-SYN1-Cre mice showed behavioral deficits including abnormal limb-clasping reflexes with progressive locomotion defects starting from ~8 weeks of age and death at ~13 weeks. Histological analysis demonstrated that the neuronal degeneration and inflammation were present in the hippocampus and in the cortex but the cerebellum only displayed increased inflammation. Importantly, we showed that neurodegeneration occurred due to stimulation of the autophagy pathway in the brain of *Ostm1*$^{lox/lox}$-SYN1-Cre. Taken together, our results demonstrated a crucial role for the *Ostm1* gene in neuronal homeostasis independent of the hematopoietic lineage and further establish physiological link of Ostm1 between the bone and the brain.

ABRÉGÉ

L'ostéopétrose maligne autosomique récessive est une maladie génétique osseuse qui résulte d'un défaut des ostéoclastes qui dérivent de la lignée hématopoïétique. Nous avons précédemment caractérisé le gène *Ostm1* responsable de la mutation spontanée grey-lethal menant à l'ostéopétrose recessive chez la souris, caractérisée par une accumulation anormale de tissu osseux. Nous avons obtenu une restauration fonctionnelle des défauts hématopoïétiques incluant les ostéoclastes dans les souris PU.1-*Ostm1-gl/gl*. Cependant, l'analyse des ces souris a suggérée un rôle primaire du gène *Ostm1* dans les cellules neuronales ceçi a ensuite été confirmé par la caractérisation d'anomalies du cerveau chez des patients porteurs de mutations affectant le gène *OSTM1*. Afin de comprendre la fonction d'*Ostm1* dans les cellules neuronales, une ablation conditionnelle d'*Ostm1* a été induite spécifiquement dans les neurones avec les souris SYN1-Cre. Les souris *Ostm1*$^{lox/lox}$-SYN1-Cre montrent des déficits comportementaux incluant des réflexes anormaux des membres, des défauts de locomotion qui progressent à partir de l'âge de ~8 semaines jusqu'à la mort des souris aux environs de 13 semaines. Des analyses histologiques démontrent que la dégénération neuronale et l'inflammation sont présentes dans l'hippocampe et le cortex, mais seul le cervelet montre une inflammation encore accrue. De manière importante, nous avons montré une stimulation de la voie de signalisation de l'autophagie dans le cerveau des souris *Ostm1*$^{lox/lox}$-SYN1-Cre, un mécanisme qui peut expliquer la neuro-dégénérescence observée. Nos résultats démontrent un rôle crucial de l'activité du gène *Ostm1* dans l'homéostasie neuronale, indépendamment de la lignée hématopoïétique, et établissent un lien physiologique os-cerveau impliqaunt le géne *Ostm1*.

Chapter1. Literature review

1.1 Bone

The bone is one of the largest organs in our body that is involved in many different functions. Bones mechanically protect and support other vital internal organs, help actions of muscle, serve as a reserve of calcium and phosphate homeostasis, and lastly, provide a platform for and support hematopoiesis (Rodan 1998).

The porous mineralized tissues of bones consist of cells, vessels and hydroxyapatite in order to carry out its various functions. The composition is well regulated by genes depending on cell type and location. There are largely two types of bones: cortical bones and a trabecular bones. The former are dense, hence account for 80% of the skeleton's mass (Hadjidakis and Androulakis 2006). The dense cortical bones have a high resistance and serve as a mechanical support at outer parts of the skeleton. On the other hand, the trabecular bones are the more elastic tissues with higher turnover rate. They comprise the inner portions of the long bones of vertebrae, pelvis and other large flat bones (Hadjidakis and Androulakis 2006). They take part in the metabolic functions such as providing initial mineral supplies (Hadjidakis and Androulakis 2006).

1.1.1 The development of bones

There are two major types of bone formation. Both types generate bones from mesenchymal progenitors. One is intramembranous ossification, a direct conversion of the tissues into calvaria. The other is endochondral ossification, in which the tissues are initially converted to cartilages. The latter process is specific to long bones and vertebral bones.

The intramembranous ossification is a classic way to form flat bones. During the intramembranous ossification, mesenchymal cells proliferate and then condense into compact nodules. They developed to become either capillaries or mature osteoblasts that produce type 1 collagen and binds to calcium phosphate (Hadjidakis and Androulakis 2006). Finally, calcified osteoid matrix is formed.

For the endochondral ossification, mesenchymal cells are activated to become cartilage cells by many paracrine factors including paired box 1 (Pax1) and Scleraxis (SF 2000). The activated mesenchyme cells condense into compact nodules that differentiate into the cartilage cells and chondrocytes. Proliferation of the chondrocytes is followed by dramatic increase of cell volume in order to produce hypertrophic chondrocytes. These cells produce collagen X and fibronectin with their original cartilage-specific extracellular matrix. The new

matrix can be mineralized by calcium carbonate. After the cartilage has been invaded by blood vessels, hypertrophic chondrocytes undergo apoptosis in order to facilitate bone modeling; while the chondrocytes undergo programmed cell death, cells surrounding the cartilage differentiate into osteoblasts and form the bone matrix.

1.1.2 Bone remodeling and homeostasis

Adult bones are dynamic tissues that constantly undergo remodelling, a process results in replacing old bones with new tissues to maintain shape, quality and size of a skeleton (Fig.1-1). The process is carried out by precisely coordinated actions of osteoclasts and osteoblasts.

Osteoblasts are bone-forming cells that are derived from multipotent mesenchymal stem cells, which have the capacity to differentiate into many different cells, such as adipocytes, chondrocytes, myoblasts, and fibroblasts. Once osteoblasts have matured, they remain on the bone surface to become flat lining cells and cluster together. Osteoblast activities are carefully regulated by both autocrine and paracrine signalling of growth factors including insulin-like growth factors (IGF) (Hadjidakis and Androulakis 2006).

Osteoclasts are multinucleated bone resorbing cells that originate from monocyte/macrophage lineage. A mature osteoclast is adherent to bones and have two functional domains: a resorptive surface, which has a ruffled border, and a basolateral membrane. The ruffled border secretes protons (H+) by H+-ATPase in order to generate a pH of 4 – 5 in resorptive lacuna (Tolar, Teitelbaum et al. 2004). The ruffled border also secretes enzymes that participate in the resorption of organic components of a bone. The basolateral membrane domain is responsible of exocytosis of degraded products by tartrate-resistant acid phosphatase (TRAP) (Tolar, Teitelbaum et al. 2004). Bone resorption is controlled by enzymes like Cathepsin K that require an acidic pH to digest organic components of bones and by proton pumps to resorb mineral matrices.

Bone mineral density is dependent on the relative functions of osteoblasts and osteocalsts. In order to maintain bone homeostasis, crosstalk between these cells is critical; when the balance between these functions is perturbed, skeletal diseases can occur. For example, if there is too much resorption, osteoporosis could occur. In contrast, no resorption could give rise to osteopetrosis.

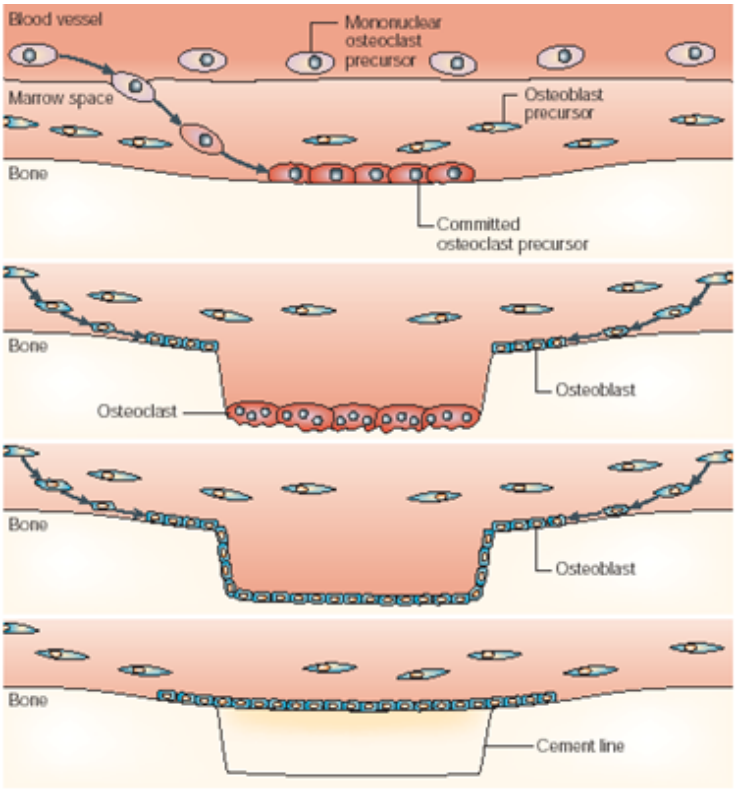

Figure 1-1: Bone remodeling. Bone remodeling is a dynamic process and is important for a normal turnover. The committed osteoclast precursors are recruited to the bone surface and mature to multinucleated osteoclasts for resorption. The osteoblasts then produce new bone tissues in the cavity lacunae. (Reprinted by permission from Macmillan Publishers Ltd. Nature Reviews Genetics (Teitelbaum and Ross 2003), copyright 2003)

1.2 Osteopetrosis

Osteopetrosis is a heterogeneous group of heritable disorders, in which there is defective bone resorption by osteoclasts. The disease was first described in humans by Dr. Albers-Schönberg. He found an increased bone density in radiography of a patient (HE 1904).

Osteopetrosis is characterized by an increase in skeletal mass and in bone density. The most common and apparent identification of the disease is by a radiographic appearance of the classic “bone in bone” appearance (Fig.1-2A). Generalized osteosclerosis is observable in addition to altered shape and structure of bones due to abnormal activities of osteoclasts and cause an increase in brittleness of bone. In severe cases, very little medullary cavity remains, resulting in hematopoietic failure. The abnormal shape of skeleton and bone can be corrected by hematopoietic stem cell transplantation (HSCT) (Fig.1-2B).

Figure 1-2: Appearance of osteopetrotic bones. (A) Classical “bone in bone” appearance in a radiograph of the forearm of an autosomal recessive osteopetrosis patient. (B) Normalized bone appearance after hematopoietic cell transplantation. The radiograph was taken two years after the treatment. (Tolar, Teitelbaum et al. 2004) (Reproduced with permission from Tolar J et al., 2004, Copyright Massachusetts Medical Society)

1.2.1 Role of the osteoclasts in osteopetrosis

Defects in osteoclasts are the main cause of osteopetrosis; these defects can be either intrinsic or extrinsic to osteoclast. Since osteoclast is of hematopoietic origin, when a defect is intrinsic, it can be rescued by HSCT (Sobacchi, Schulz et al. 2013).

All defects, either intrinsic (mutation in the cell itself) or extrinsic (mutation in microenvironment), can be classified as two types. One corresponds to a failure in osteoclast differentiation, in which there is a complete absence of mature osteoclasts (osteoclast poor osteopetrosis). The other results in formation of mature osteoclasts but with impaired resorptive function (osteoclast rich osteopetrosis) (Teitelbaum 2000, Teitelbaum and Ross 2003, Sobacchi, Schulz et al. 2013).

Several transcriptional factors have been described as essential for osteoclast differentiation. PU.1 is the earliest known factor that affects osteoclastogenesis (Fig.1-3). It regulates the synthesis of receptors for macrophage colony stimulating factor (M-CSF). The M-CSF is primarily generated by stromal cells and osteoblasts to regulate the differentiation of osteoclast precursors from monocytes and hematopoietic stem cells (Fig.1-3)(Tolar, Teitelbaum et al. 2004).

A mouse model of PU.1-/- mouse, knockout of *mcsf*, and a *op/op* mouse, insertional mutation in *mcsf*, both lack osteoclasts development (Wiktor-Jedrzejczak, Bartocci et al. 1990, Tondravi, McKercher et al. 1997). Another factor that is important in the early osteoclastogenesis is microphthalamia-associated transcription factor (MITF) family. A *mi/mi* mouse, which has mutation within *Mitf* gene, synthesizes osteoclasts, but they fail to fuse or have abnormal ruffled border and unable to resorb the bone matrix (Hodgkinson, Moore et al. 1993).

Osteoclast precursors differentiate into mature osteoclasts through signalling induced by RANKL-RANK interactions (Fig.1-3)(Tolar, Teitelbaum et al. 2004). They express the receptor activator of nuclear factor κappa-B (RANK) receptors on their membrane. When the receptor activator of nuclear factor kappa-B ligands (RANKLs) on the osteoblast membrane interact with RANK receptors on the osteoclast membrane, several signalling pathways including mitogen-activated protein kinases (MAPK), Phosphatidylinositol-4,5-bisphosphate 3-kinase (PI-3K) and nuclear factor kappa-light-chain-enhancer of activated B cells (NFkB) are induced (Lee and Kim 2003). These signalling pathways promote the differentiation of osteoclast precursors into mature osteoclasts. When those genes are mutated, osteopetrosis occurs. For example, both RANKL Knockout

and RANK Knockout mice models develop osteopetrosis due to the absence of osteoclasts (Kong, Yoshida et al. 1999, Li, Sarosi et al. 2000).

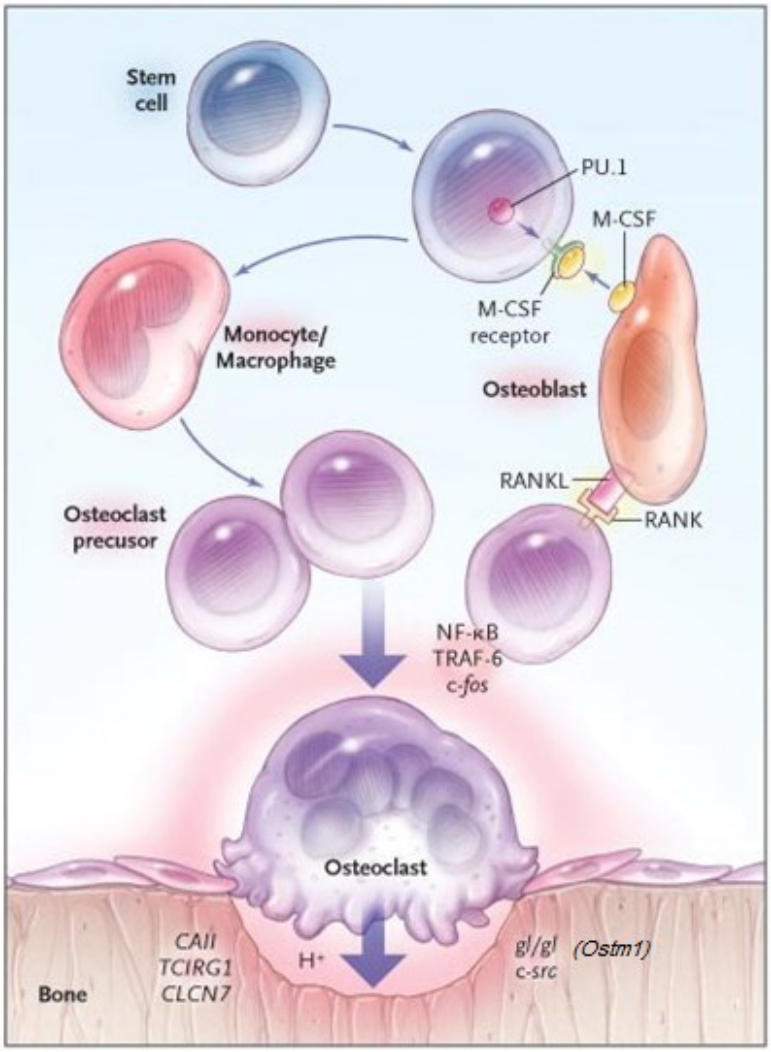

Figure 1-3: Molecules affecting osteoclast differentiation and maturation. PU.1 is the earliest factor required for differentiation of osteoclast and other hematopoietic cells. M-CSF then regulates the differentiation. RANK-RANKL interaction is also very important in the last stages of osteoclast differentiation as defect in this interaction prevents osteoclast formation. c-src, *CAII*, *TCIRG1*, *CLCN7* and *OSTM1* also contribute at the later stages after the differentiation. (Tolar, Teitelbaum et al. 2004) (Reproduced with permission from Tolar J et al., 2004, Copyright Massachusetts Medical Society)

Not only are the genes responsible for osteoclast differentiation crucial, but the genes for functioning of matured osteoclast are also important. For the resorptive function of osteoclast, it is critical to have normal ruffled border which acts as a resorptive surface of the osteoclast. Grey-lethal mice, which have spontaneous mutations in the *Ostm1* gene, have increased number of osteoclasts and underdeveloped ruffled border(Rajapurohitam, Chalhoub et al. 2001). Another important factor for the development of osteopetrosis is the filamentous actin and $\alpha_v\beta_3$ integrin. They are involved in the attachment of osteoclasts to bone matrix (Fig.1-4). Furthermore, failure in degradation of bone matrix also results in osteopetrosis. As stated above, the organic matrix is degraded by enzymes including cathepsin K while hydroxyapatite is degraded in the acidic resorption lacunae. (Fig.1-4). Therefore it is important to maintain an acidic environment to have proper degradation of bone matrices. A cathepsin K knockout mice(Saftig, Hunziker et al. 1998) and an *oc/oc* mice (mice with mutations in *Atp6i*, gene important for ATP-dependent osteoclast-specific vacuolar proton pump (V-ATPase))(Li, Chen et al. 1999, Scimeca, Franchi et al. 2000) give rise to osteopetrosis due to malfunction of osteoclasts (Sobacchi, Schulz et al. 2013).

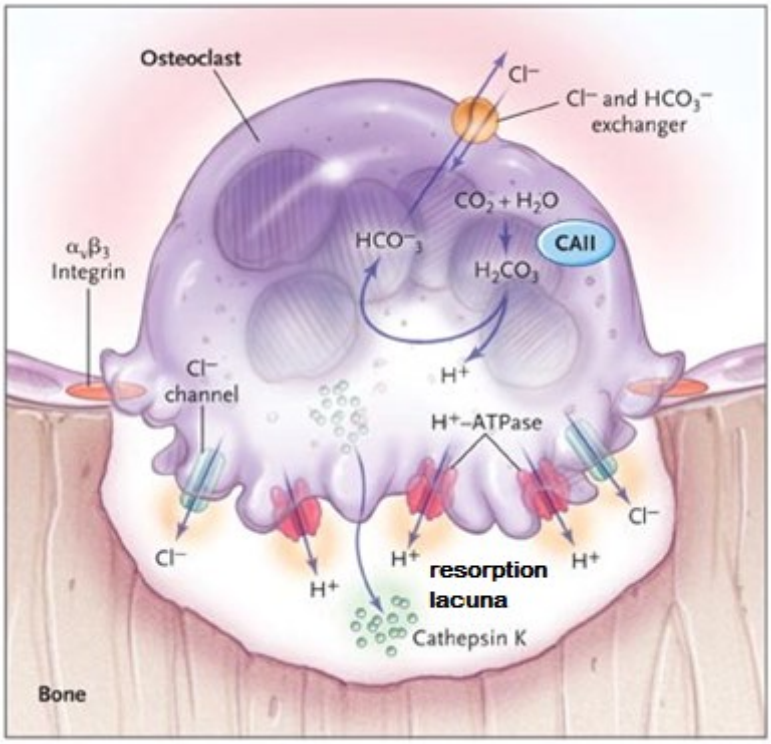

Figure 1-4: Osteoclast Physiology. To form a resorption lacuna, osteoclasts stick to the bone surface by $\alpha_v\beta_3$ integrin. Proton(H^+) is secreted to resorption lacuna by H^+-ATPase on ruffled border and Cl^- is secreted by chloride channel to maintain electroneutrality. Enzymes including Cathepsin K are also secreted to the resorption lacuna for degradation of a bone matrix (Tolar, Teitelbaum et al. 2004). (Reproduced with permission from Tolar J et al., 2004, Copyright Massachusetts Medical Society)

1.2.2 Forms of osteopetrosis in human

Osteopetrosis can be classified as three forms: infantile or malignant autosomal recessive osteopetrosis (ARO), intermediate autosomal recessive osteopetrosis (IRO) and autosomal dominant osteopetrosis (ADO) (Baik, Picetti et al.).

The disorder described by Dr. Albers-Schönberg was later categorized as the ADO. ADO is the most frequent form of osteopetrosis with the incidence of 5 in 100,000 (Del Fattore, Cappariello et al. 2008). ADO has milder phenotypes and almost all patients with ADO have a normal life expectancy.

IRO is a recessive osteopetrosis with intermediate severity. It is much less frequent with only few cases reported so far. IRO forms mostly by the loss of carbonic anhydrase (CAII) function (Del Fattore, Cappariello et al. 2008). CAII is responsible of producing H^+ ion for acidification (Fig.1-4). Since the acidification is a key mechanism involved in the process of resorption by osteoclasts, malfunction in CAII activity leads to osteopetrosis. However, the CAII deficiency also causes severe renal tubular acidosis and brain calcifications as well as osteopetrosis. Because renal defect seems to be more severe than the osteopetrotic symptoms, the IRO is not often considered as a typical osteopetrosis (Sobacchi, Schulz et al. 2013).

ARO is also called malignant infantile osteopetrosis. The symptoms develop soon after or before birth and are lethal. It is a rare disorder with an incidence of 1:250,000 with higher incidence in some regions such as Costa Rica, the Middle East, the Chuvash Republic of Russia, and Västerbotten in northern Sweden

(Sobacchi, Schulz et al. 2013). The majority of ARO patients have defects intrinsic to osteoclasts which can be cured by HSCT. The mutations causing ARO are spontaneous mutations in *TCIRG1, CLCN7, OSTM1 and SNX10*. These mutations lead to osteoclast-rich AROs (Sobacchi, Schulz et al. 2013). On the other hand, mutation in *TNFSF11* which results in inactive RANKL cause defects that are extrinsic to osteoclasts leading to osteoclast-poor AROs (Sobacchi, Schulz et al. 2013). The osteoclast-rich AROs have defective endosomal and/or lysosomal vesicle trafficking which result in osteoclasts with poorly developed ruffled border and no bone resorption (Sobacchi, Schulz et al. 2013). ARO patients have life-threatening symptoms including growth retardation, hypocalcaemia, hematological and/or visual impairment, neurological central nervous system (CNS) defects in addition to osteopetrotic phenotypes (Sobacchi, Schulz et al. 2013).

1.3 ARO

ARO is caused by two different types of mutations: mutations affecting the ruffled border formation and those affecting the osteoclastogenesis.

Mutations in *TCIRG1, CLCN7, OSTM1* and *SNX10* result in malformation of ruffled border. The functional osteoclast has a ruffled border in which H^+ ions and

secretory lysosomal enzymes are released for resorption. Before the formation of the ruffled border, osteoclasts must attach to the surface of the bone. This process is facilitated by filamentous actin and $\alpha_v\beta_3$ integrin. The opposite side of the ruffled border, the basal membrane is involved in exocytosis of degraded products. The polarization of membrane, maintained by highly specific vesicular trafficking pathways, is critical as it is required for ruffled border formation (Coxon and Taylor 2008).

In order for normal differentiation and maturation of osteoclast to proceed, RANK-RANKL interaction is very important (Fig.1-3). When there is mutation in either RANK or RANKL, there is absolutely no maturation of osteoclast leading to ARO (Kong, Yoshida et al. 1999, Li, Sarosi et al. 2000).

1.3.1 *TCIRG1*

Mutations in *TCIRG1* are a common cause of ARO as 50-53% of the patients exhibit a mutation in this gene (Sobacchi, Schulz et al. 2013). *TCIRG1* encodes a3 subunit of V0 complex, one of the two complexes of V-ATPase (Del Fattore, Cappariello et al. 2008) (Fig1-5).

V-ATPase is a multimeric protein in lysosome, composed of V0 subunit for proton pumping, and V1for generatingATP (Fig.1-5). The V-ATPase pumps the protons into and acidifies endosomes and lysosomes. Researchers suggested that V0 complex is involved not only in proton pumping but also in vesicle trafficking. The subunits of V-ATPase have been found to be critical for synaptic vesicle fusion in neurons of *drosophila melanogaster* and also for insulin secretion in pancreatic β-cells through vesicle fusion in pancreas of mice (Hiesinger, Fayyazuddin et al. 2005, Sun-Wada, Toyomura et al. 2006).

The *TCIRG1* mutation causes defective V-ATPase which causes a defect in the generation of the acidic environment and in the delivery of V-ATPase as well as the delivery of lysosome. The tethering of lysosomes at the ruffled border is essential for the ruffled border formation (Sobacchi, Schulz et al. 2013). Therefore, mutation in *TCIRG1* causes defects in vesicle trafficking in addition to impaired proton pumping, giving rise to ARO.

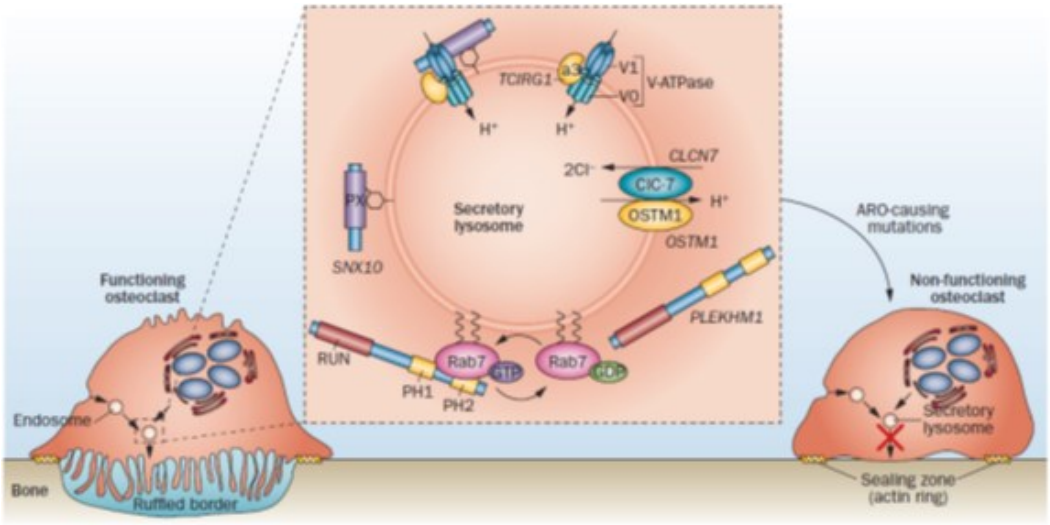

Figure 1-5: Mechanisms underlying osteoclast-rich ARO. Mechanism involved in transport of secretory lysosome to the secretary surface is essential for ruffled border formation and development of functioning osteoclasts. *TCIRG1* encodes for V0 subunit of V-ATPase which is responsible for proton pumping. *CLCN7* and *OSTM1* encode for ClC-7 chloride channel in the secretary lysosome. *SNX10* seems to regulate trafficking of V-ATPase. (Reprinted by permission from Macmillan Publishers Ltd. Nature Reviews Endocrinology (Sobacchi, Schulz et al. 2013), copyright 2013)

1.3.2 *CLCN7*

Mutation in *CLCN7* is the second most common cause of osteopetrosis.

Homozygous mutation results in 13-16% of ARO cases while heterozygous mutation leads to ADO (Cleiren, Bénichou et al. 2001, Kornak, Kasper et al. 2001, Sobacchi, Schulz et al. 2013). *CLCN7* encodes for Cl^-/H^+ exchange transporter 7 (ClC-7) found in late endosomes and lysosomes (Sobacchi, Schulz

et al. 2013)(Fig.1-5). Together with its function as an exchanger, ClC-7 is responsible of balancing the charges of ions.

Recently, it was suggested that ClC-7 participates in trafficking by controlling chloride ion concentration. A mouse model with point mutation in *Clcn7* give rise to osteopetrosis with defective ClC-7, uncoupled Cl^- conductor. The mouse shows decrease in luminal chloride ion concentration in the lysosome but normal lysosomal pH. It was suggested that luminal chloride ion concentration may modulate endosomal calcium ion channels and efflux (Saito, Hanson et al. 2007). In addition to this, ClC-7 deficient mouse have enlarged late endosome and lysosome in renal proximal tubule cells and accumulation of lysosomal storage material in hippocampal and cortical neurons (Wartosch, Fuhrmann et al. 2009). In conclusion, *CLCN7* mutations give rise to the malfunctioning of osteoclast by the defective lysosomal trafficking, which results in abnormal ruffled border formation, rather than by defective acidification.

Interestingly, the *Clcn7* systemic knockout mice showed severe neurodegeneration as well as osteopetrotic and hematopoietic defects. Brain phenotypes in osteopetrosis are described with other mutation. However, it is important that in $Clcn7^{-/-}$ mice, they were primary phenotypes of the

osteopetrosis. Firstly, unlike retinal neuron culture from *oc/oc* mice, retinal neuron culture of *Clcn7* knockout mice showed neurodegeneration (Kasper, Planells-Cases et al. 2005). Additionally, histology analysis showed accumulation of electron-dense material in neurons with microglial activation and astrogliosis in *Clcn7*$^{-/-}$ mice (Kasper, Planells-Cases et al. 2005). This shows that ClC-7 has a critical role in osteoclast and autonomous functions in other tissues including brain.

1.3.3 *OSTM1*

OSTM1, the main interest in our lab and this thesis, is another gene that is responsible of ARO when mutated. It is very rare as only 2-6% of patients have *OSTM1* mutation (Sobacchi, Schulz et al. 2013). *OSTM1* has 6 exons and encodes for Osteopetrosis associated trans-membrane protein 1 (Ostm1) which is a type I trans-membrane protein (Chalhoub, Benachenhou et al. 2003). Ostm1 is the β-subunit of ClC-7 (Lange, Wartosch et al. 2006). ClC-7 is required to export Ostm1 from ER to endosome/lysosome (Stauber and Jentsch 2010). However, in grey-lethal mice, ClC-7 protein concentration is greatly reduced while the mRNA level is not affected (Lange, Wartosch et al. 2006). Therefore, Ostm1 is thought to be involved in protein stabilization of ClC-7 protein.

1.3.4 *SNX10*

SNX10 is a newly discovered gene that is involved in ARO (Aker, Rouvinski et al. 2012, Pangrazio, Fasth et al. 2013). It is a member of a protein family called sorting nexins characterized by phox homology (PX) domain, a phospholipid binding motif that targets protein to endosomes (Worby and Dixon 2002). There is evidences that PX domain in sorting nexin 10 (SNX10) interacts with V1D subunit of V-ATPase (Fig. 1-5) and SNX10 could regulate the trafficking of V-ATPase (Chen, Wu et al. 2012). This suggested that *SNX10* mutation leads to ARO by the disruption in trafficking of V-ATPase. In addition to this, all reported *SNX10* mutations that are associated with ARO are in the PX domain (Pangrazio, Fasth et al. 2013). In conclusion, there is high possibility that mutation in *SNX10* cause ARO by defects involved in trafficking of V-ATPase.

Like patients with CLCN7 or OSTM1 mutations, patients with SNX10 mutations also display brain defects. It was reported that a boy from an Iraqi family with an infantile osteopetrosis history had ARO with SNX10 mutation. The patient showed osteopetrosis features with hematological defects as well as brain atrophy, external hydrocephalus and corpus callosum hypoplasia (Mégarbané, Pangrazio et al. 2013).

1.4 *OSTM1* human patients

Human patients with *OSTM1* mutations show signs of ARO within 1 year and have severe symptoms with short life expectancy (Sobacchi, Schulz et al. 2013). The *OSTM1*-related ARO is caused by nonsense mutation, frameshift, splice-site mutation, or microdeletion (Ott, Fischer et al. , Quarello, Forni et al. 2004, Ramírez, Faupel et al. 2004, Pangrazio, Poliani et al. 2006, Maranda, Chabot et al. 2008). The *OSTM1*-related ARO patients showed common osteopetrotic phenotypes such as bone-in-bone appearance, increase in bone density and bone marrow failure with defective osteoclasts with no resorptive activity (Maranda, Chabot et al. 2008, Mégarbané, Pangrazio et al. 2013). Patients develop anemia, hepatosplenomegaly and cytopenia with major liver failure (Maranda, Chabot et al. 2008, Mégarbané, Pangrazio et al. 2013). In addition to typical features of osteopetrosis, patients showed neurological impairment. (Maranda, Chabot et al. 2008)

1.4.1 Osteopetrosis and the central nervous system

Disruptive bone remodeling affects not only the bone marrow formation but can also affect skull thickness and formation of cranial foramina where nerves, spinal cord and blood vessels pass through (Steward 2003). As a secondary result, CNS function is greatly affected as patients often develop hydrocephalus, growth

retardation, and cranial nerve compression leading to blindness and deafness (Steward 2003).

Mutations in the *TCIRG1* and the *SNX10* seem to have neurological phenotypes secondary to the osteopetrosis. When the *TCIRG1*- and the *SNX10*-related ARO patients receive HSCT before the CNS defects develop, the patients do not develop CNS related defects (Pangrazio, Fasth et al. 2013, Sobacchi, Schulz et al. 2013).

In contrast, patients with *CLCN7* or *OSTM1* mutation develop neurological defect not secondary to the bone phenotype. The neuron culture of *Clcn7* knockout mice showed neurodegeneration and lysosomal storage defect. Despite the rescue of bone phenotype by transgene carrying TRAP-*Clcn7*, the transgenic mice still shows the neurological defect with retinal degeneration (Kasper, Planells-Cases et al. 2005). This supports that the neurological defect is independent of the bone defects. Previously in our lab, it was shown that neurological defects in *Ostm1*-related ARO in *gl/gl* mice was not secondary as rescue of bone phenotype by transgene revealed neurological impairment of the mice (Héraud, Griffiths et al. 2014).

1.4.2 Cases study

The first patient with *OSTM1*-related ARO was reported by Chalhoub et al. in 2003 (Chalhoub, Benachenhou et al. 2003) and the pathology characterized by Quarello P et al. in 2004 (Quarello, Forni et al. 2004). In our lab, we have studied another patient with *OSTM1*-related ARO. The patient was firstly admitted with feeding problems, irritability and poor visual contact at the age of 3 months and died at 1 year. Sequence analysis from patient genomic DNA detected a substitution of G to T generating a stop codon at position 256 in exon 1 of *OSTM1* (Fig.1-6A) (Maranda, Chabot et al. 2008). This mutation as the one in Chalhoub et al. (Chalhoub, Benachenhou et al. 2003) results in a shorter protein without the transmembrane domain such that it will most likely be degraded or secreted (Lange, Wartosch et al. 2006). The *OSTM1* RNA was detectable only with increased polymerase chain reaction (PCR) cycles and was decreased 20- to 50 fold (Fig.1-6B) indicating mRNA decay. Primary osteoclasts were differentiated from patient's blood and multinucleated but non-functional osteoclasts were observed (Maranda, Chabot et al. 2008). The normal development of osteoclasts corresponds to a role for *OSTM1* in bone resorption function of osteoclasts instead of a role in osteoclast differentiation.

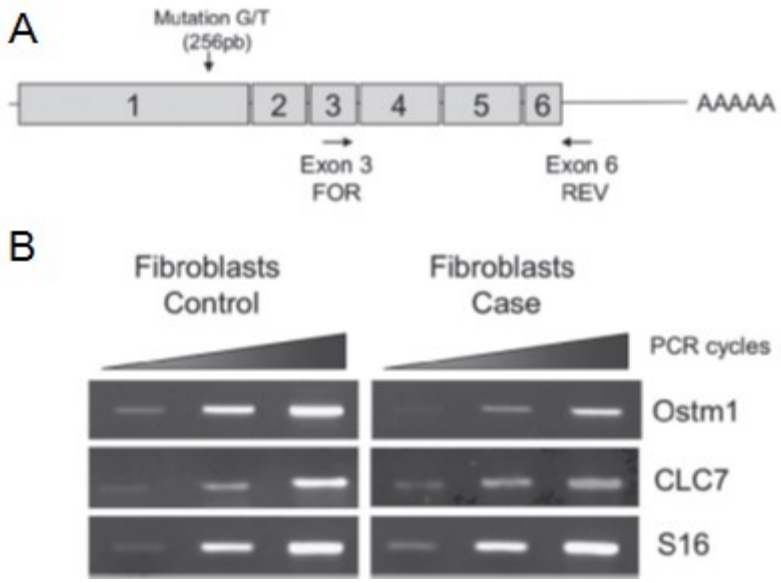

Figure 1-6: Expression analysis. (A) Scheme of OSTM1 RNA with mutation site. Primers used for RT-PCR are shown on the scheme. (B)RT-PCR results showing that *Ostm1* RNA expression level is decreased in patient's fibroblasts compared to control and only detectable with increased number of PCR cycles. (Reproduced by permission from John Wiley and Sons, Journal of Bone and Mineral Research (Maranda, Chabot et al. 2008), Copyright © 2008 ASBMR)

This patient showed poor visual contact, delayed development and also generalized seizure from 4 months of age. Common ARO symptoms such as hepatosplenomegaly, anemia, thrombocytopenia and increase in bone density were found. However, there was no optic and auditory nerve compression (Maranda, Chabot et al. 2008). This finding was noticeable because other ARO patients can have visual and/or hearing loss which is secondary to the abnormal bone deposition causing the compression of nerves. From these findings, it was

suggested that the neurological symptoms in this *OSTM1*-related ARO patient may not be secondary to the defective bone remodeling.

The cerebral magnetic resonance imaging (MRI) results of this patient further support the hypothesis that the defect in the brain is primary and showed delayed myelinization, cerebral atrophy, bilateral atrial subependymal heteropias and subdural frontal hematoma (Fig.1-7)(Maranda, Chabot et al. 2008). The cerebral atrophy found in the patient may be a direct result of the *OSTM1* mutation. Furthermore, the heteropias are the first evidences of defective neuronal development due to this *OSTM1* mutation.

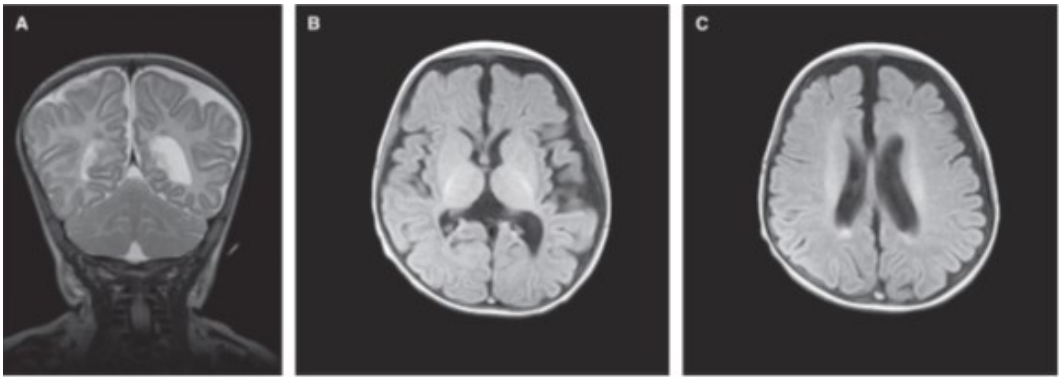

Figure 1-7: Cerebral MRI of the *OSTM1*-related ARO patient. (A) Coronal T2 showing subependymal heterotopias, delayed myelinization and global atrophy (B) Axial T1 showing subependymal heterotopias (C) Axial T1 showing subependymal heterotopias (Reproduced by permission from John Wiley and Sons, Journal of Bone and Mineral Research (Maranda, Chabot et al. 2008), Copyright © 2008 ASBMR)

In addition to the findings from this patient, studies in *gl/gl* mouse model also supports the direct role of *OSTM1* in neuronal physiology which will be discuss further in the thesis.

1.5 The grey-lethal mouse

Grey-lethal mouse (*gl*) is a mouse model with a spontaneous recessive mutation in *Ostm1* and previously in our lab, we have found that mouse *Ostm1* gene is 83% homologous to human *OSTM1* (H 1936, Chalhoub, Benachenhou et al. 2003). Similar to *OSTM1*-related ARO patients, *gl/gl* mice have high bone density due to the defective resorption function of osteoclast (Rajapurohitam, Chalhoub et al. 2001). The *gl/gl* mice die at 3-4 week of age because of osteopetrosis and hematopoietic defects (Rajapurohitam, Chalhoub et al. 2001, Chalhoub, Benachenhou et al. 2003).

The wild-type (WT) *Ostm1* locus covers approximately 23kb of genomic DNA and includes 6 exons and 5 introns (Fig.1-8). The spontaneous *gl* mutation is due to a deletion of ~7.5kb including start codon and the whole exon 1 with 3kb of the first intron of the *Ostm1* gene (Fig.1-8). The deletion results in the absence of Ostm1 RNA and protein in *gl/gl* mice.

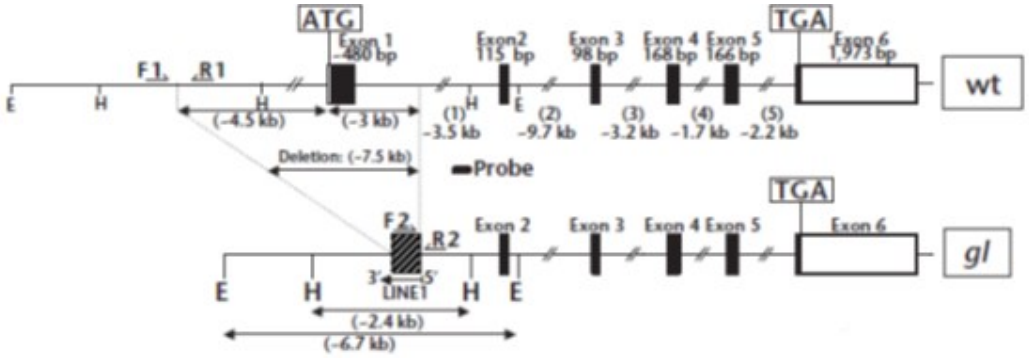

Figure 1-8: Genomic structure of the wild-type and the *Ostm1* gene. Wild-type *Ostm1* gene is approximately 23kb with 6 exons. The *gl* mutation corresponds to a deletion of 7.5kb which covers the exon 1 with the start site and 3kb of first intron. Reprinted by permission from Macmillan Publishers Ltd: Nature Medicine (Chalhoub, Benachenhou et al. 2003), copyright (2003)

In wild-type mice, the *Ostm1* gene is expressed not only in bone but also in many different tissues including brain, kidney, spleen, and liver. The expression in melanocytes and in the brain is particularly high. However, the *gl/gl* mice expression of *Ostm1* was undetectable in all of these tissues. Interestingly, the absence of *Ostm1* in melanocytes gives *gl/gl* mice its distinct grey coat color due to pheomelanin granules clumping in melanocytes (H 1936).

The *gl/gl* mice have slightly more multinucleated osteoclasts compared to the wild-type. (Rajapurohitam, Chalhoub et al. 2001) Yet, they are not functional because of defective cytoskeletal reorganization leading to abnormal ruffled border formation.(Rajapurohitam, Chalhoub et al. 2001)

Due to the defective osteoclast, bone remodelling is impaired which results in high bone density (Fig.1-9). Severely reduced bone marrow with high bone density and calcified trabeculae accumulation was observed in the long bones of *gl/gl* mice (Rajapurohitam, Chalhoub et al. 2001). Growth and development of vertebrae was also reduced with very little medullary space (Rajapurohitam, Chalhoub et al. 2001).

The absence of bone marrow results in hematopoiesis defects. Mild anemia and lymphopenia is observed in *gl/gl* mice. The B-cell population is reduced and T-cell population is altered with reduced thymus size (Pata, Héraud et al. 2008). From the fluorescence-activated cell sorting (FACS) analysis of thymic T cell populations, a depletion of $CD4^+CD8^+$ double positive cells was observed with double negative $CD4^-CD8^-$ cells comparable to that of the wild-type mice (Pata, Héraud et al. 2008). The altered population double positive and double negative cells results 4-~5-fold increase in $CD4^+$ or $CD8^+$ single positive cells.

1.5.1 PU.1 transgenic mice

Since multinucleated osteoclasts are developed in *gl/gl* mice, we generated *Ostm1* transgenic mice with TRAP promoter to target the committed osteoclast precursors. However TRAP-*Ostm1-gl/gl* showed similar osteopetrotic phenotype

with homologous *gl/gl* mice (Pata, Héraud et al. 2008). Therefore, Ostm1 expression in late committed osteoclast precursor is not sufficient for development of functional osteoclast with ruffled border.

Secondly, for rescue of both the bone and the hematopoietic defects, PU.1 promoter was selected to target hematopoietic multipotent stem cells (Fig.1-4). Since the regulatory region of PU.1 is large, bacterial artificial chromosome (BAC) was used in order to include the whole ~37kb of 5' PU.1 regulatory sequence and 18kb of 3' sequence (Pata, Héraud et al. 2008).

First of all, PU.1 BAC clones containing *Tbp1* were isolated from 1295v mouse pBelo11 BAC genomic library(Pata, Héraud et al. 2008). The *Tbp1* gene was removed by homologous recombination with a construct containing two homologous regions that are 31kb apart, generating BAC PU.1Δ *Tbp1* (Fig.1-9A)(Pata, Héraud et al. 2008). Then another construct with *Ostm1* ORF and polyA sequence was inserted in the BAC PU.1Δ *Tbp1* and co-integrated to remove *PU.1* genomic sequence (Fig.1-9A)(Pata, Héraud et al. 2008). The PU.1-*Ostm1* BAC was microinjected to generate transgenic founders. Finally, the PU.1-*Ostm1-gl/gl* mice were obtained by crossing the foundering colony with *gl/+* mice. The PU.1-

Ostm1-gl/gl mice were rescued from the osteopetrotic and the hematopoietic phenotypes (Fig.1-9B) and lived past 3 weeks (Pata, Héraud et al. 2008).

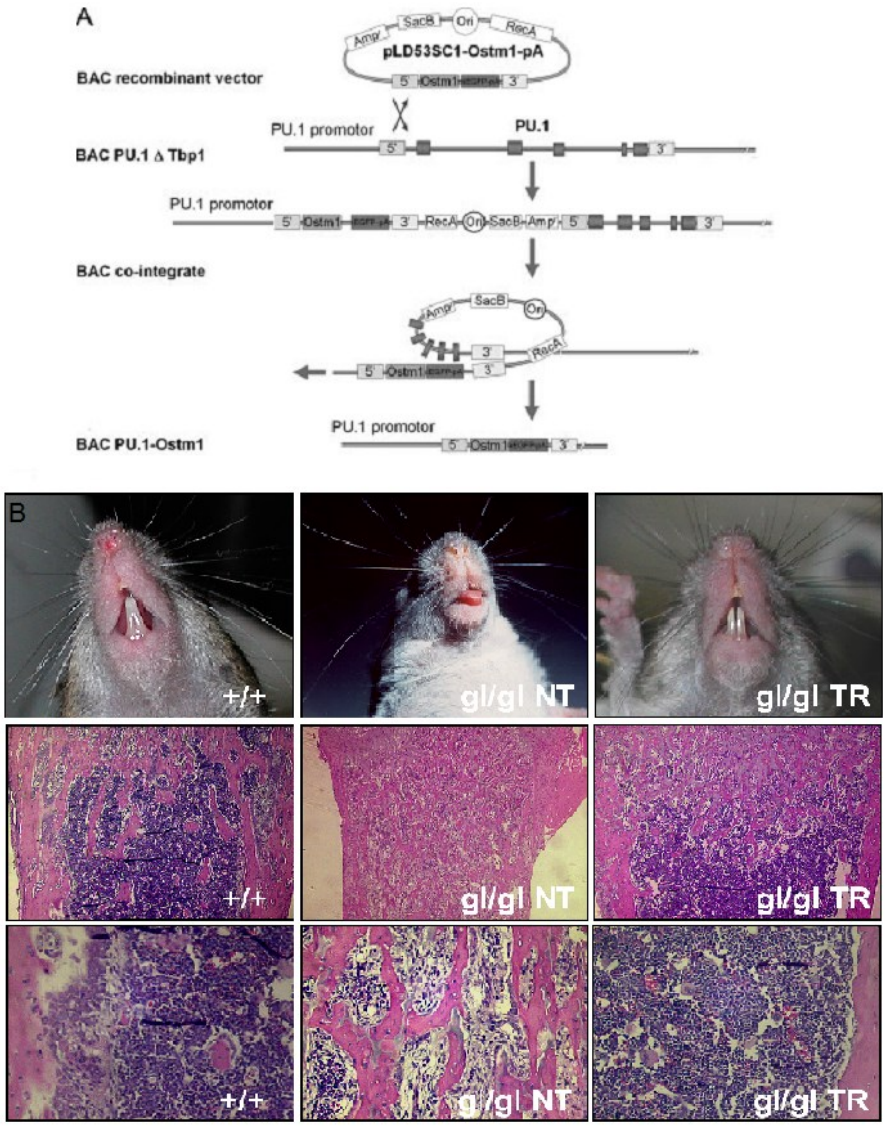

Figure 1-9: Generation of PU.1-*Ostm1* transgene and rescue of osteopetrosis in PU.1-*Ostm1-gl/gl* mice. (A) A scheme of generating the BAC *PU.1-Ostm1* from BAC *PU.1* Δ*Tbp1* (B) Rescue of osteopetrosis in PU.1-*Ostm1-gl/gl* (*gl/gl* TR) compared to non-transgenice mice (*gl/gl* NT). Top panel shows tooth eruption and two bottom panel shows the development of medullary space on bone with Hematoxylin and Eosin (H&E) staining. (Pata, Héraud et al. 2008)

In conclusion, unlike *CLCN7* knockout mice, whose symptoms can be corrected with TRAP-*Clcn7* at the later stage of osteoclast development, *gl/gl* mice phenotype is not rescued by transgene expressed only at the later stage. This suggests that *Ostm1* mutation has impacts from earlier stage in the osteoclast development and also in a wider spectrum including hematopoiesis.

Even though PU.1-*Ostm1* corrected the bone and hematopoietic phenotypes, the PU.1-*Ostm1-gl/gl* mice still have a shorter lifespan of 6-7 weeks compared to 2 years in wild-type mice. Knowing that the Ostm1 expression is high in brain, brain histology of the PU.1-*Ostm1-gl/gl* mice was analyzed. Inflammation, including astrogliosis and microglial activation, was observed with severe neurodegeneration in the brain and the retina (Fig.1-10). In the neurons, abnormal storage of cellular metabolites such as carbohydrates, lipids and ubiquitinated proteins and accumulation of autophagosomes were observed (Héraud, Griffiths et al. 2014).

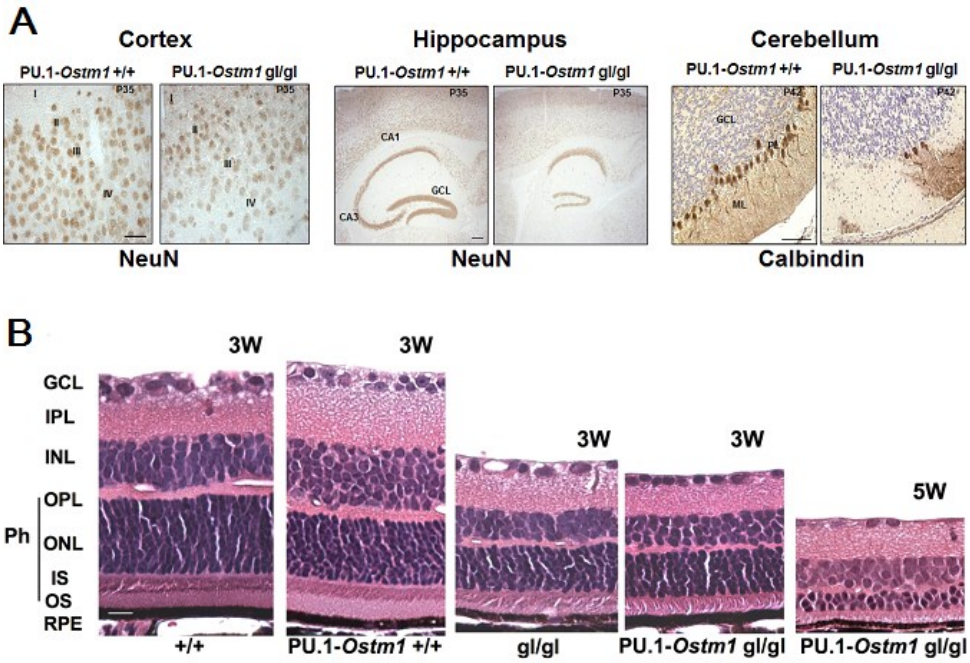

Figure 1-10: Neurodegeneration and retinal degeneration in *gl/gl* and PU.1-*Ostm1-gl/gl*. (A) cortical and hippocampal neurodegeneration in PU.1-*Ostm1-gl/gl* is detected with NeuN staining on brain sections. Loss of purkinje cells in cerebellum was visualized with Calbindin staining on brain sections. (B) Retinal degeneration in PU.1-*Ostm1-gl/gl* and *gl/gl* stained with H&E on retina sections. (Héraud, Griffiths et al. 2014)

These findings in PU.1-*Ostm1-gl/gl* mice, with support of brain defect found in *OSTM1*-related ARO patients(Maranda, Chabot et al. 2008), suggest the role of Ostm1 in brain physiology apart from a role for Ostm1 in hematopoietic lineages including the osteoclast.

1.5.2 Functional rescue of neuronal defects in double transgenic mice

Ostm1 is expressed in different cell types in the brain with major expression in neurons and astrocytes. Thus, the primary cells responsible for the brain phenotype in the PU.1-*Ostm1- gl/gl* mice were investigated. We have first generated GFAP (glial fibrillary acidic protein)-*Ostm1* transgenic founders to target astrocytes(Brenner and Messing 1996, Nolte C 2001) and SYN1 (Synapsin 1)-*Ostm1* for targeting neurons(Zhu, Romero et al. 2001) (Fig.1-11A)(Héraud, Griffiths et al. 2014). Secondly, in order to test functional rescue, double transgenic PU.1-*Ostm1*-GFAP-*Ostm1-gl/gl* and PU.1-*Ostm1*-SYN1-*Ostm1-gl/gl* were produced. Only PU.1-*Ostm1*-SYN1-*Ostm1-gl/gl* showed full rescue of brain phenotype (Fig.1-11B) in addition to normal hematopoiesis including osteoclasts development (Héraud, Griffiths et al. 2014). Ostm1 was found to have a primary and autonomous role in neuronal physiology independently of hematopoietic lineages and exclude most likely astrocytes as the cell type responsible for the neurodegenerative phenotype.

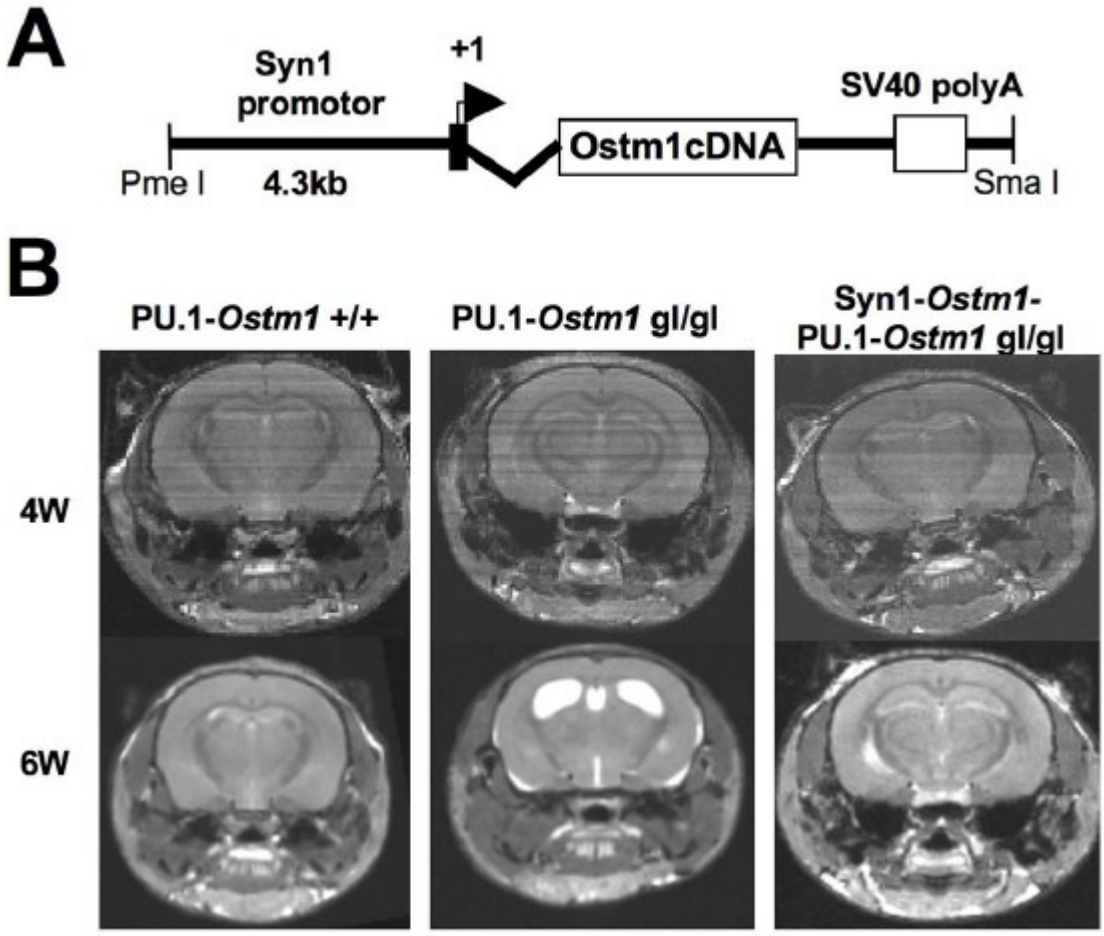

Figure 1-11: rescue of neurodegeneration by SYN1-*Ostm1* transgene.

(A) Scheme of SYN1-*Ostm1*. The transgene contains 4.3kb of rat Synapsin 1 promoter with *Ostm1* cDNA. (B) MRI scan of 4-week-old and 6-week-old PU.1-*Ostm1*-+/+, PU.1-*Ostm1-gl/gl*, and PU.1-*Ostm1*-SYN1-*Ostm1-gl/gl*. The MRI scan shows the complete rescue of brain defect in PU.1-*Ostm1*- SYN1-*Ostm1-gl/gl* which was observed in PU.1-*Ostm1-gl/gl*. (Héraud, Griffiths et al. 2014)

Hypothesis and approach

The study of human *OSTM1*-related ARO patient revealed symptoms of significant neurological phenotypes, leading us to investigate the primary role of OSTM1 in brain. From the previous studies in our lab of PU.1-*Ostm1-gl/gl* mice and other analysis of transgenic mice, we have hypothesized that Ostm1 has a critical role in neuronal physiology. To test this hypothesis, we used the genetic Cre-lox system to exclude any effect from other tissues where Ostm1 is expressed. We generated a conditional *Ostm1* allele to be able to induce specific *Ostm1* ablation in neurons with the neuronal-specific SYN1-Cre deleter mice. We then used cellular and molecular approaches to analyze the conditional knockout mice in relation with neuronal physiology.

Chapter 2: Materials and Methods

2.1 Mice

All mice were provided with laboratory chow and tap water ad libitum and maintained in a 12-hour light/dark cycle at temperature of 22-26°C. All the protocols and procedures were followed guidelines of the Canadian Committee for Animal Protection and were approved by the local Institutional Animal Care and use Committee (see Appendix 1).

All mice were backcrossed on a C57BL/6 background for more than ten generations to obtain genetic identity.

2.1.1 *Ostm1* floxed mice

Ostm1 floxed mice were produced in our lab by inserting loxP sites in introns flanking exon 5 region of *Ostm1* gene. This was to mimic mutations in human patients. When Cre recombinases recognize the flanking region, the region was excised and resulted in an Ostm1 protein without the transmembrane domain. These recombined proteins would be secreted out of cells. KO237 and KO195 lines were generated and KO195 was analysed in more detail.

2.1.2 Synapsin-Cre recombinase mice

The mouse strain B6.Cg-Tg(Syn1-cre)671Jxm/J was obtained from the Jackson Laboratory. This strain expresses Cre recombinase in neuronal cells that express Synapsin1. The promoter used for the strain was also used to generate SYN1-*Ostm1* transgenic mice, discussed below.

2.1.3 Grey-lethal mice

The mouse strain GL/Le *d*/^{J} +/+ *gl* was obtained from the Jackson Laboratory. The strain was maintained by brother x sister mating for more than 190 generations.

2.1.4 SYN1-*Ostm1* mice

SYN1-*Ostm1* mice were produced in our lab as previously described (Héraud, Griffiths et al. 2014) There were two lines generated, 214 and 215, and the former with 2 copy numbers of the transgene was used in our experiments.

2.1.5 Genotyping of Mice

DNA from tail tips was isolated by salt preparation. The tails were first digested in digestion buffer (50mM Tris-HCl (pH8), 100mM EDTA (pH8), 100mM NaCl, 1% SDS) with 150µg of Proteinase K for overnight at 55°C. DNA was then

precipitated in 5M NaCl and 100% EtOH followed by re-suspension in TE buffer (100mM Tris-HCl (pH8), 1mM EDTA (pH8)).

0.1 – 0.5µg of DNA was added to the PCR reaction buffer (10mM Tris-HCl pH 8.3, 50mM kCl and 1.5mM $MgCl_2$; 10% DMSO added only for SYN Ostm1 assay) with polymerase, 12µM primers (see table 1) and 1.25mM dNTP for PCR reaction. PCR cycling conditions were 35 cycles as follows: 94°C for 30 seconds, 63°C for 30 seconds, 72°C for 30 seconds and10 minute of elongation at 72°C. Resulting amplicons were visualized in 1.5% 1X TBE (89mM Tris, 89mM Boric Acid and 2mM EDTA) agarose gels stained with Ethidium Bromide (EtBr).

KO Osmt1 PCR assay was done to detect the floxed allele (200bp amplicon), the wild-type allele (100bp amplicon) and the Delta allele (100bp amplicon). Ostm1 assay was done to determine the mutated *gl* allele (330bp amplicon) and the wild-type allele (236bp amplicon). SYN transgene assay and Cre recombinase assays give one amplicon each at 450bp and at 500bp respectively.

2.1.6 Crosses

SYN1-Cre mice obtained from Jackson laboratory was crossed with $Ostm1^{lox/lox}$ mice to generate F1 heterozygous *Ostm1* floxed with SYN1-Cre then female F1

was crossed with male heterozygous *Ostm1* floxed mice to obtain *Ostm1*$^{lox/lox}$-SYN1-Cre.

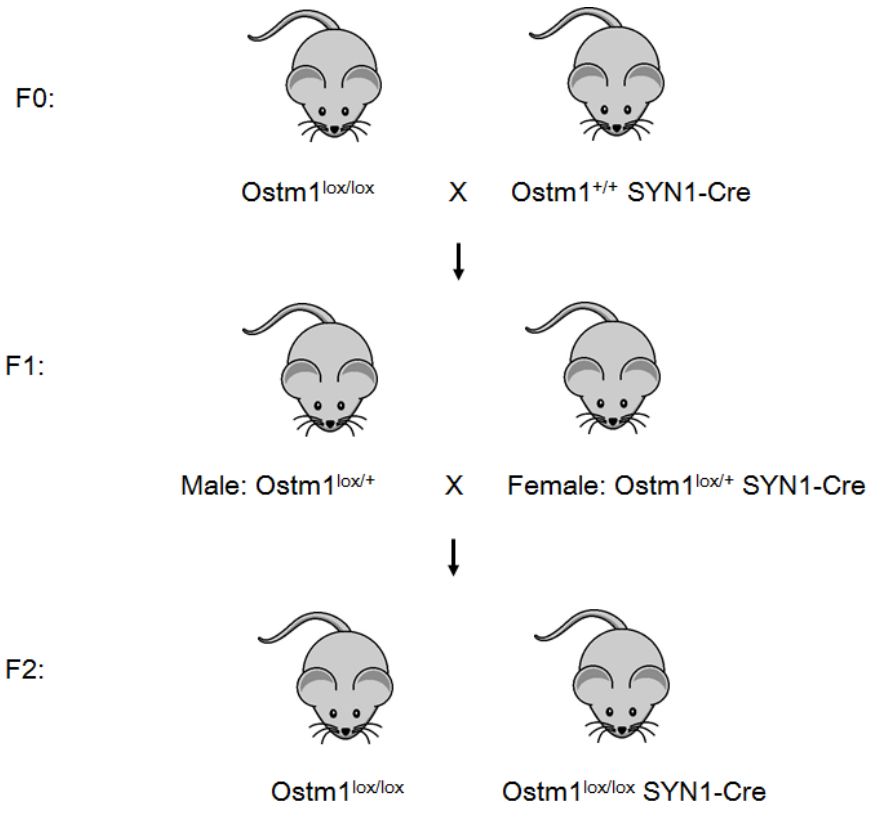

Figure 2-12: Mating scheme for *Ostm1*$^{lox/lox}$-SYN1-Cre mice. *Ostm1*$^{lox/lox}$ mice were crossed with SYN1-Cre mice (from Jackson Laboratory) to obtain female heterozygous *Ostm1* floxed mice containing SYN1-Cre. Only female heterozygous *Ostm1* floxed mice with SYN1-Cre was used for crossing because male SYN1-Cre mice produces recombination in germline cells.(Rempe, Vangeison et al. 2006) The female *Ostm1*$^{lox/+}$ SYN1-Cre mice were mated with male heterozygous *Ostm1* floxed mice.

2.2.1 Hippocampal neuronal culture

2.2.1.1 Isolation of Neurons

Hippocampus was isolated from the mice brain and kept in sterile ice-cold 1X HBSS. The hippocampus was minced into small pieces then treated either with 0.25% Trypsin, for P0 ~ P1 tissues, or with 0.25% Papain, for adult tissues, for 15 minutes at 37°C. After washing with pre-warmed 1X HBSS, the supernatant was replaced with Neuronal Plating Medium (Neurobasal medium supplemented with B27 (50X, Invitrogen), 2mM L-glutamine, 100U/ml of penicillin, and 1 µg/ml of streptomycin). The dispersed cells were counted and adjusted to a maximum of 3.5×10^5 cells/ml. 1ml of this cell solution was plated to each well of Poly-L-Lysine coated 24-well plate or on cover slips.

2.2.1.2 Maintaining Neuronal cultures

Neuronal cultures were not disturbed for 2 days *in vitro*. On day 2, 0.5ml of medium was carefully replaced with Neuronal Maintenance Medium (Minimum Essential Medium (Invitrogen) supplemented with 0.6% glucose and N2 (100X, Invitrogen)). From day 3, the cultures were maintained in Neuronal Maintenance Medium for at least 7 days.

2.3 Molecular analysis

2.3.1 Southern blot

2.3.1.1 DNA digestion and analysis

Genomic DNA of mice was digested with restriction enzyme BamHI for overnight at 37°C. The digested DNA fragments were loaded on a 0.7% 1X TBE agarose gel and migrated for overnight at 60V.

The gel with well-separated DNA fragments was treated with 1M NaCl, 0.5M NaOH solution in order to denature the double stranded fragments to single strands. The samples were then neutralized with 3M NaCl, 0.5M Tris HCl (pH7.5) solution. The DNA was then transferred to a nylon membrane by capillary method using 20X SSC (3M NaCl, 0.3M sodium citrate, pH7.0) for overnight. Crosslinking was done under UV light for 15 minutes.

2.3.1.2 Radioactive Probe labelling and membrane hybridization

Genomic DNA of 500bp corresponding exon 5 of mouse *Ostm1* was used as template and amplified by PCR using the same thermal cycling as genotyping. Primers used were: Sonde 5 For (5'-TCTGTGTGAGGGCTTGACTG-3'); Sonde 5 Rev (5'-AACACGATGTAGCCTTGACTTC-3'). The PCR product was separated by agarose gel and electroeluted. The isolated DNA was then precipitated in 100% EtOH and 0.2M NaCl at -20°C.

100ng of the probe DNA was used as a template in nick translation by DNA polymerase I for making ^{32}P dCTP labelled probe. Before hybridization with the probe, membrane was incubated with 100ug/ml Salmon Sperm DNA in hybridization buffer (5X SSC: 1.5M NaCl, 75mM sodium citrate; 5X Denhart:1% ficoli, 1% polyvinylpyrroplidone, 1% BSA; and 0.1% SDS) 4 hours at 65°C water bath in order to prevent unspecific hybridization. The radioactive probe was added in the buffer to the pre-hybridized membrane and incubated overnight at 65°C.

The membrane was washed with solution II (0.3M NaCl, 15mM sodium citrate, and 0.1% SDS) then with solution III (0.03M NaCl, 1.5mM sodium citrate and 0.1% SDS) to remove nonspecific binding and exposed to a film in -80°C for 1-7 days depending on intensity of signal.

2.3.1.3 Determination of recombination efficiency

The intensity of floxed *Ostm1* band and recombined *Ostm1* band was quantified by measuring pixels with Image Quant Version Build software (Molecular Dynamics). The recombination efficiency in brain was calculated by ratio between the two intensities.

2.3.3 mRNA expression

2.3.3.1 RNA isolation

Cells in cultures or tissues from mice were homogenized with Trizol for dissociation of nucleoprotein complexes. When the homogenized sample was mixed with chloroform, the mixture was separated into an aqueous and an organic phase. RNA was precipitated using isopropanol from the aqueous phase, washed with 75% Ethanol and dissolved in DEPC treated water.

2.3.3.2 Reverse transcription PCR (RT-PCR) analysis

cDNA was produced from total RNA by reverse transcription. The 1g of total RNA was first treated with DNase at room temperature for 15 minutes to remove any trace of remaining DNA. The DNase treated RNA was incubated with 10mM poly dT primer and 2.5mM dNTP at 65°C for 10 minutes so the primer can be annealed to the poly A tails of RNA. Then 100units of M-MuLV Reverse Transcriptase in RT M-MuLV buffer (50mM Tris-HCl, 75mM KCl, 3mM $MgCl_2$, 10mM DTT pH8.3) was used for reverse transcription which was carried at 42°C in 1 hour. After the reaction, the enzyme was inactivated at 70°C for 15 minutes. PCR analysis was carried out with 1/5 diluted cDNA in RT-PCR reaction buffer (10mM Tris-HCl (pH8.3), 50mM KCl, 1.5mM MgCl2) with specific primers (see

table 2). The PCR cycles were 35 cycles of 94°C for 30 seconds, 63°C for 30 seconds, 72°C for 30 seconds followed by 10 minutes at 72°C for elongation.

2.3.3.3 Real-time PCR (qPCR) analysis

qPCR analysis was carried out by MX3005 Stratagene using SYBR Green Mastermix (Qiagen, Mississauga, Ontario, CA). 1µ of the diluted cDNA and primers (see table 3) were mixed with 25µl reaction mix. Ribosomal S16 was used as internal control.

Firstly, the reaction mix was at 95°C for 15 minutes to denature cDNA and activate Hot Star Taq DNA polymerase in the mix. Then, 40 cycles were carried out as follows: 95°C for 30 seconds, 60°C for 30 seconds, and 72°C for 30 seconds.

2.4 Biochemical analysis

2.4.1 Antibodies & reagents

The following antibodies and reagents were used for the biochemical analysis. Primary antibodies used were: mouse anti-β-actin (Sigma), rabbit anti-LC3 (Sigma), rabbit anti-ATG5 (Sigma).

Secondary antibodies used were: Horseradish Persoxidase (HRP) labeled goat anti-mouse and goat anti- rabbit IgG (BioRad).

2.4.2 Protein extraction and quantification

Tissues obtained from dissections were homogenized with 1ml of 1X RIPA buffer (150mM NaCl, 1% NP-40, 0.5% sodium deoxycholate, 0.1% SDS, and 50mM Tris, pH8.0) for 100mg of tissue with protease inhibitors (1mM PMSF, 1mM β-glycerophosphate, 2mM Sodium Orthovanadate, 1/1000 of Protease Inhibitor Cocktail (sigma)). After homogenization, the samples were incubated on ice for 30 minutes then centrifuged at 12,000RPM for 10 minutes at 4°C to remove debris. The extracted proteins were quantified using the Bradford Assay.

2.4.3 SDS-polyacrylamide gel electrophoresis

5% staking gel and various percentages of resolving gel depending on the size of protein were prepared. On the each well, 15μg of protein (boiled for 5 min in sample buffer: 62.5mM Tris-HCl pH 6.8, 2% SDS, 10% glycerol, 0.002% bromophenol blue and 5% β-mercaptoethanol) was loaded. Electrophoresis was performed in running buffer (25mM Tris, 190mM Glycine, and 0.1% SDS) at 100V for 30 minutes then at 150V until ladders were well separated.

2.4.4 Western blot

The protein gels were transferred to Polyvinylidene Fluoride (PVDF) membranes at a constant current of 300mA for 1.5 hour. The transfer buffer (25mM Tris and 190mM Glycine) was kept cold to prevent denaturation of proteins during the transfer.

The membrane was then blocked with 5% skim milk in 1X TBST (20mM Tris, 137mM NaCl, and 0.1% Tween; pH7.6). Primary antibody (1:5000 for β-actin and 1:1000 for others) was diluted in 3% BSA in 1X TBST then added to the membrane. The incubation was for overnight at 4°C. Membranes were washed in 1X TBST. Secondary antibody (1;10,000 in 5% skim milk in 1X TBST) incubation was done for 1 hour in room temperature followed by washing. The membranes were exposed using ECL Western Blotting Detection kit (Amersham GE Healthcare). At needs of stripping, the membranes were incubated in stripping solution (2% SDS, 62.5mM Tris-HCl (pH6.7), 0.6% β-mercaptoethanol) to remove antibodies.

2.5 Behaviour analysis

2.5.1 Inverted Grid test

Animals were tested for three trials with no previous training. For each trial, the mouse was put on the grid (bars spaced 1.5 cm apart) in a vertical position. The grid was then reversed upside down at a height of 25 cm above a padded cushion. The latency until the animal fell from the grid was recorded, the cut-off time was 5 minutes.

2.5.2 Balanced beam test

At 4 weeks of age, animals were first tested on a 25 mm beam (80cm in length) to allow them to learn that traversing the beam would result in the safety of the enclosed box. The 60W white light was placed behind the start position to encourage the animal to walk down. Three trials were conducted, separated by 10 minutes. If the animal stopped on the beam, or attempted to reverse direction, it was gently prodded to continue or reoriented in the proper direction. This procedure was repeated on days two and three, except the beam widths used were 12.5 and 6 mm, respectively. All trials were recorded to DVD and then manually scored for latency in crossing the beam and for paw slips (paws placed on the side of the beams). At 8 and 12 weeks, animals were retested on the 12.5 and 6 mm (but not the 25 mm) beam, using the same procedure as for week 4.

2.5.3 Rotarod test

Rotarod model 755 from IITC Life Science (Woodland Hills, CA) was used. On day 1, mice were first familiarized and trained on the test apparatus. Each mouse was trained by 3 trials of 120 sec. Starting speed for each trial was 4 revolutions per minute (RPM), and this was increased over the course of the trial to a maximum of 6 RPM on trial 1, 12 RPM on trial 2 and 24 RPM on trial 3. If an animal fell, it was replaced and allowed to complete the trial (120 sec maximum). The duration of the inter-trial interval (Kong, Yoshida et al.) was 30 minutes.

Testing was conducted on day 2 and each mouse had 3 trials (30 minute ITI) each with a maximum duration of 300 seconds. The start speed was 4 RPM and was increased to a maximum speed of 25 RPM for each trial. Time spent on the rotarod was recorded.

2.5.4 Novel object recognition test

The test was conducted in 4 identical arenas constructed of grey, opaque Plexiglas measuring 44.5 x 44.5 x 49.5 cm, located in a sound-attenuating room illuminated by 260W red light bulbs. The test objects consisted of (1) pyramids, which consisted of three dice glued together in pyramidal shape, and (2) glass bottles roughly identical in width and height to the dice. On day 1, animals were

transported in their home cages to an antechamber to the testing room and familiarized for 30 minutes. They were then placed, individually, into one of the arenas, each of which contained two pyramids that were placed along a diagonal of the open field, offset 10 cm from the corners. Animals were allowed to freely explore for 10 minutes. They were then returned to their home cages for 60 minutes, and returned to the arena that now contained one pyramid (the familiar object) and one glass bottle (the novel object) for 10 minutes. The positions of the novel and familiar objects were counterbalanced across animals. The arenas and objects were thoroughly cleaned with Periguard antiseptic between animals.

All trials were recorded to DVD with an infrared camera, the recordings of which were analyzed with the Top Scan 2.0 tracking system (Clever systems, Reston, Virginia, USA). The software measured the number of visits and cumulative duration in which the animals' nose was within a circle with a diameter equal to the width of the pyramid object. Visits and duration were then converted to percent preference scores: [Novel/(Novel + Familiar)] X 100. A preference score above 50% positive value indicates more exploration of the novel object; 50% indicates no preference, whereas a negative ratio indicates more exploration of

the familiar object. The Top Scan 2.0 system was also programmed to calculate distance travelled (i.e., total distance (cm) travelled in the arena during a trial).

2.6 Histochemical analysis

2.6.1 Antibodies & reagents

Following antibodies and reagents were used for the biochemical analysis. Primary antibodies used were: mouse anti-NeuN (Chemicon), mouse anti-GFAP (Sigma). Secondary antibodies used were: Horseradish Peroxidase (HRP) labeled goat anti-mouse and goat anti- rabbit IgG (BioRad).

2.6.2 Tissue embedding & sectioning

Mice perfusion and tissues fixation were done for tissues embedding in paraffin and sectioning. After anesthesia by 2.5% avertine (in 1X PBS (137mM NaCl, 2.7mM KCl, 4.3mM Na_2HPO_4, and 1.47mM KH_2PO_4) pH7.5, 0.018µl per gram of mouse), the mouse was perfused and fixed with 4% PFA. The brain was removed and incubated in 4% PFA at 4°C overnight. The fixed tissue was embedded in paraffin then sectioned for 5µm.

2.6.3 Immunohistochemistry

Paraffin was removed by xylene followed by rehydration of sections using ethanol with decreasing percentage to water from 100% to 70%. Heat induced epitope retrieval was done using citrate buffer (10mM Sodium Citrate, pH6) at 95 °C for 20 minutes. The sections were rinsed with PBST (0.1% Tween in 1XPBS) followed by blocking with 10% Normal Goat Serum for 30 minutes at room temperature. Sections were then incubated with primary antibody (1:100 for NeuN and 1:400 for GFAP diluted in 1% Normal Goat Serum) overnight at 4°C. Unbound antibodies were removed by incubation for 2 minutes with PBST for 3 times at room temperature. Quenching was done with 3% H_2O_2 in PBS to block peroxidase followed by secondary antibody (1:100 dilution) incubation. The signal was developed with DAB peroxidase substrate kit (Vector) and the sections were counterstained in Hematoxylin for 0.5 – 5 minutes depending on the intensity.

2.7 Statistical Analysis

Values are expressed as mean ±SEM. Unpaired two-sample Student's t test was used for statistical analysis with $P<0.05$ considered significant.

Table 1: Primers for PCR analysis

assay	Name	Sequence
KO Ostm1	gl 5' For 3	5'-AATAGCCAGGGTTGCACAGAGAGT-3'
	gl EX5 qR	5'-GCTGGTTTACAATTAGTAAGTG-3'
	gl 3' qR5	5'-TTTCACAGGGATAGTATTTTGATGC-3'
Ostm1	gl For 1	5'-CCTCTGGAAGACTAATACTTGCTG-3'
	gl For 2	5-GCTACATCTGGGTCCTTTCG-3'
	gl Rev 1	5'-GCCTGGAACAGAGCAAAGC-3'
	gl Rev 2	5'-CGCTTGCTTTTGTCTGTTACCTTTGTGTTC-3'
SYN1 Transgene	SYN For 1	5'-ATTTAGTACCGCCGACAGAGCCTT-3'
	RGH Rev 1	5'-AGTTGGGATGCCCTCACACTAGAA-3'
Cre Recombinase	Cre For	5'-AATGCTTCTGTCCGTTTGC-3'
	Cre Rev	5'-CGGCAACACCATTTTTTCTG-3'

Table 2: Primers for RT-PCR analysis

assay	Name	Sequence
β-actin	β-actin For	5'-TGACGATATCGCTGCGCTG-3'
	β-actin Rev	5'-ACATGGCTGGGGTGTTGAAG-3'
Ostm1	RT Ostm1 Ex 3 For	5'-CCTGCTTTGAGCATAACCTGC-3'
	RT Ostm1 Ex 6 Rev	5'-CTGCAGTCCCAACTTTCGTGAG-3'
Cre Recombinase	iCre For	5'-CCTGGTCTGGACACAGTG-3'
	iCre Rev	5'-TTGCCCCTGTTTCACTATC-3'

Table 3: Primers for qPCR analysis

assay	Name	Sequence
S16	qS16 For	5′-GCTACCAGGGCCTTTGAGATG-3′
	qS16 Rev	5′-AGGAGCGATTTGCTGGTGTGC-3′
Ostm1	qOstm1 For 1	5′-GTGGTTGCTGTGTCTGTGTTC-3′
	qOstm1 Rev 1	5′-CAGGAGACTTCCGCCACAG-3′

Chapter 3: Results

3.1 Generation of synapsin conditional knockout allele

Grey-lethal mice have very short life span due to the Autosomal Recessive Osteopetrosis. Previously, PU.1-*Ostm1-gl/gl* mice were generated to correct the hematopoietic defect of the grey-lethal mice. Although the PU.1-*Ostm1-gl/gl* transgene had extended the life span to 6-7 weeks, the transgenic mice died due to neurological defects (Héraud, Griffiths et al. 2014). The full rescue of brain defect in PU.1-*Ostm1*-SYN1-*Ostm1-gl/gl* suggested that the brain defect is specifically due to the loss of function of Ostm1 in neurons. Therefore, we have generated *Ostm1*$^{lox/lox}$-SYN1-Cre mice to further analyze the *Ostm1* function in neuronal physiology.

Synapsins are a multigene family of neuron-specific phosphoproteins, found most abundantly in synaptic vesicle proteins (Fdez and Hilfiker 2006). They bind to synaptic vesicles to maintain a reserve pool at the presynaptic nerve terminal (Greengard 1993, Hilfiker 1999). They are also known to regulate the release of synaptic vesicle (Greengard 1993, Hilfiker 1999). SYN1 was selected because it is expressed in all differentiated neurons (Melloni and Degennaro 1994) and carries out recombination in the neurons. The Cre expression with rat Synapsin I promoter has Cre function detected as early as E12.5 in brain, spinal cord, and

dorsal root ganglion (DRG) (Zhu, Romero et al. 2001). The Cre expression continues in neurons of adult mice (Zhu, Romero et al. 2001).

In order to obtain *Ostm1*$^{lox/lox}$-SYN1-Cre mice, *Ostm1* floxed mice are first obtained (Fig.3-1). LoxP sites were introduced in the *Ostm1* locus of embryonic stem (ES) cells, by homologous recombination, flanking the *Ostm1* exon 5. Exon 5 contains the transmembrane domain of Ostm1 and hence the absence of exon 5 will result in a truncated protein which is secreted or degraded (Lange, Wartosch et al. 2006). Neo selection cassette flanked with frt sites was inserted between loxP site and exon 5 (Fig.3-1). The recombined ES cells were selected by Neo selection marker then injected into blastocysts. The chimeric mice were obtained and crossed to obtain mice with the recombinant allele. In order to remove the Neo selection marker, the recombinant mice were crossed with FLPeR mice expressing flippase activity that induce recombination of frt sites. Finally the *Ostm1*$^{lox/lox}$ mice were crossed according to the mating scheme (Fig.2-1) to obtain *Ostm1*$^{lox/lox}$-SYN1-Cre mice to be analyzed.

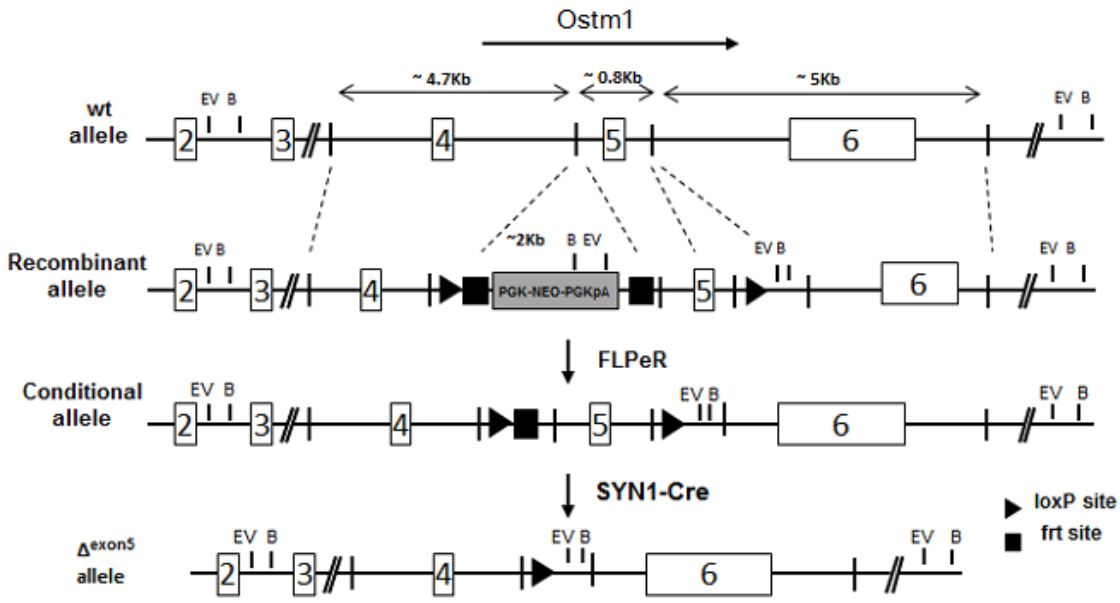

Figure 3-13: Generation of conditional allele of *Ostm1*. LoxP sites and neo selection marker with frt sites were inserted by recombination into WT *Ostm1* allele to generate recombinant allele. The conditional allele, exon 5 flanked with loxP sites, are generated by excision of Neo marker by flippase. Finally, Δ^{exon5} allele is generated by SYN1-Cre.

3.2 Efficiency and specificity of recombination

Since *gl* defect is recessive, the recombination efficiency of the *Ostm1*$^{lox/lox}$-SYN1-Cre mice must be higher than at least 50% to mimic *gl* mutation. Therefore, the efficiency was carefully examined both at the DNA and RNA levels.

3.2.1 Recombination in DNA level

Firstly, in order to examine the specificity of recombination, DNA extracted from different tissues underwent PCR amplification. The null allele (Δ^{exon5}) only

appeared in DNA extract from neurons, brain, and spinal cord (Fig.3-2B) where SYN1-Cre expressed.

Southern blot was used to analyze the specificity and the level of recombination in brain and spinal cord. DNA extracts from different tissues were digested with BamHI restriction enzyme to generate specific fragments according to the genotype (Fig.3-2A). The intensity was compared and the percentage of recombination by production of Δ^{exon5} in brain was 27% (Fig.3-2B). Since total brain extracts were used and neurons represent only ~35% of total brain cells in the mouse (Allen and Barres 2009), the estimated percentage of recombination in neurons of $Ostm1^{lox/lox}$-SYN1-Cre was ~77%.

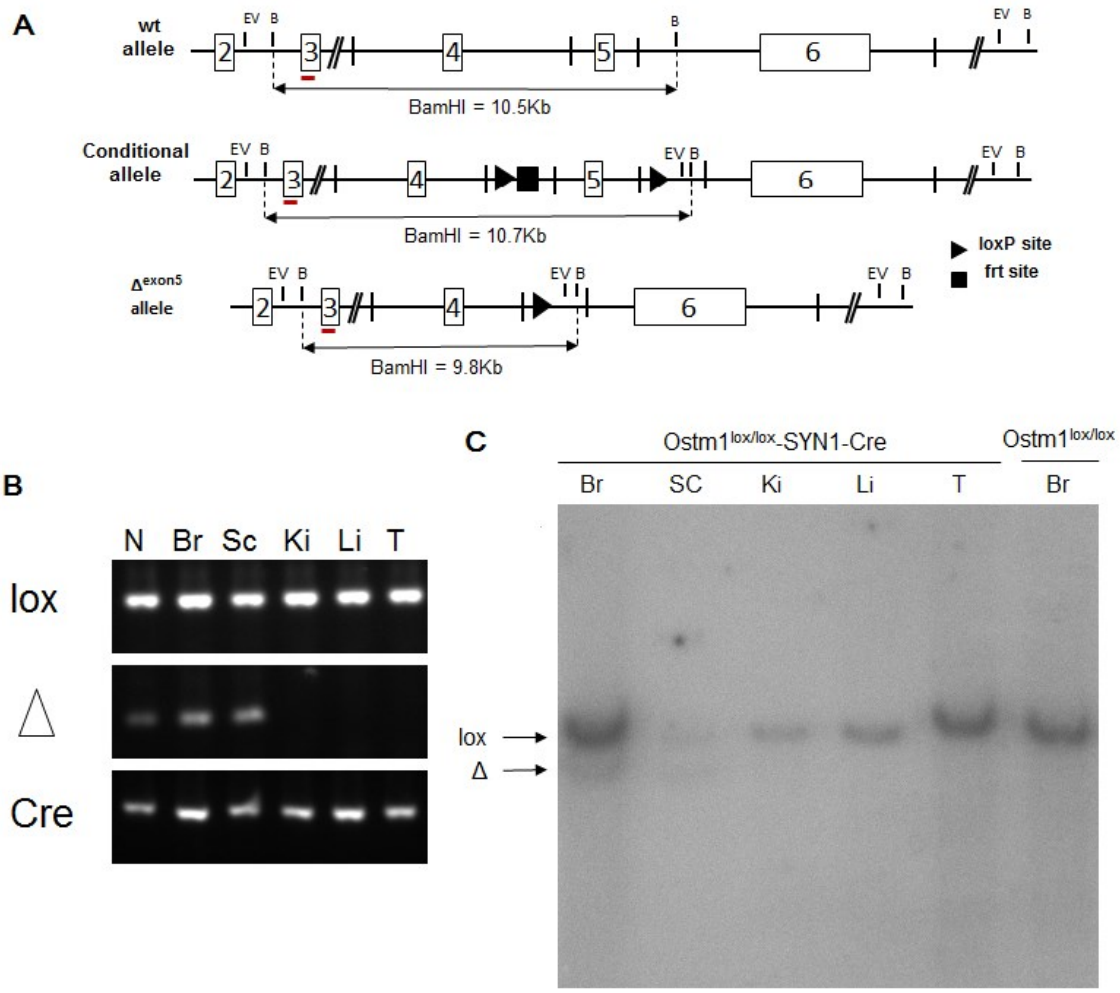

Figure 3-2: recombination efficiency evaluated by PCR and southern blot analysis. (A) Scheme showing different sized product after BamHI digestion. Red band under exon 3 indicates probe used to visualize the product. (B) PCR result showing specificity of recombination. 5-week-old mice were analyzed. (C) Southern blotting result showing the 10.7kb (floxed Ostm1) and 9.8kb (Δ^{exon5}) band following recombination. 5-week-old mice were analyzed. (N=Neuron, Br=brain, SC=spinal cord, Ki=Kidney, Li=Liver, T=Tail)

The PCR analysis and Southern blot results demonstrated specificity of recombination in neuronal cells with an efficiency of ~77% which is in a range that can mimic Ostm1 loss of function in *gl/gl* mutant mice.

3.2.2 Conditional *Ostm1* expression

Knowing that recombination efficiency was adequate, the level of *Ostm1* RNA expression was analyzed. The RT-PCR analysis showed expression of the specific Δ^{exon5} RNA only in the brain and in the spinal cord (Fig.3-3A), demonstrating again the specificity of recombination. In the RNA extract of the 5-week-old *Ostm1*$^{lox/lox}$-SYN1-Cre whole brain, the expression of *Ostm1* was decreased to 52% compared to the control mice (Fig.3-3B), quantified by qPCR. All of the cell types in brain express *Ostm1* and 68% of the expression is from neurons. Therefore the RNA expression of Ostm1 in neurons was decreased to 35%.

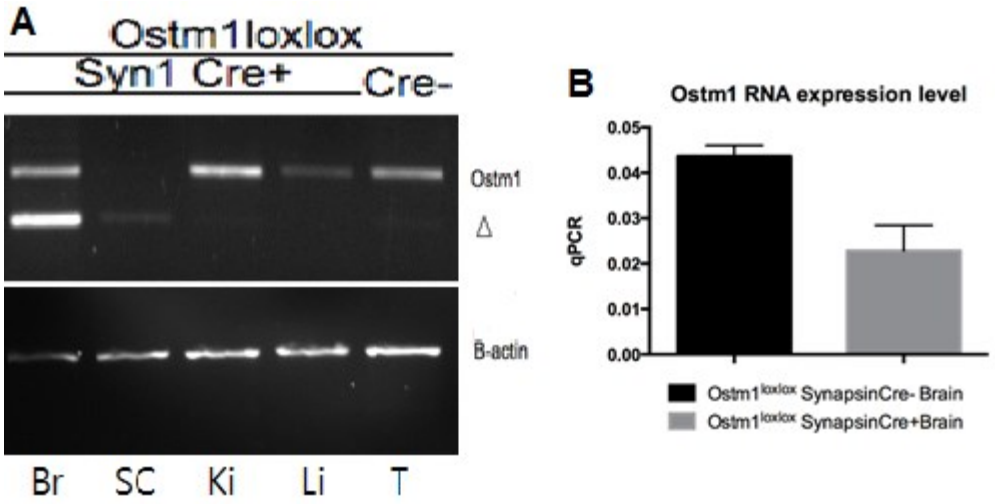

Figure 3-314: Decrease in Ostm1 RNA expression. (A) cDNA from different tissues of 5-week-mice were amplified with exon 3 and exon 6 primers. Due to excision of exon 5, null allele shows shorter band (Δ). (B) cDNA from brain of 5-week-old mice were amplified by qPCR. The Ostm1 RNA level was decreased to 52% of control.

This analysis demonstrated strong efficiency and specificity of recombination in *Ostm1*$^{lox/lox}$-SYN1-Cre mice, herein phenotypic analysis of these mice was undertaken.

3.3 Phenotypic analysis of *Ostm1*$^{lox/lox}$-SYN1-Cre mice

The SYN1 conditional knockout mice had a longer life span of 12-14 weeks compared to the grey-lethal mice (3 weeks of life expectancy) and the PU.1-*Ostm1-gl/gl* mice (6-7 weeks) analyzed by Kaplan-Meier survival analysis (Fig.3-4A). The apparent behavioural deficits in *Ostm1*$^{lox/lox}$-SYN1-Cre compared to control littermates were observed from 9 weeks of age. Tremors were the first deficit observed and other deficits such as abnormal limb-clasping reflexes (Fig.3-4C) and defective locomotion followed. There was also a progressive loss of weight possibly due to the behaviour defects that lead to challenges in eating. The loss of weight was observable from week 10, the time point after the behaviour defects were observed (Fig.3-4B).

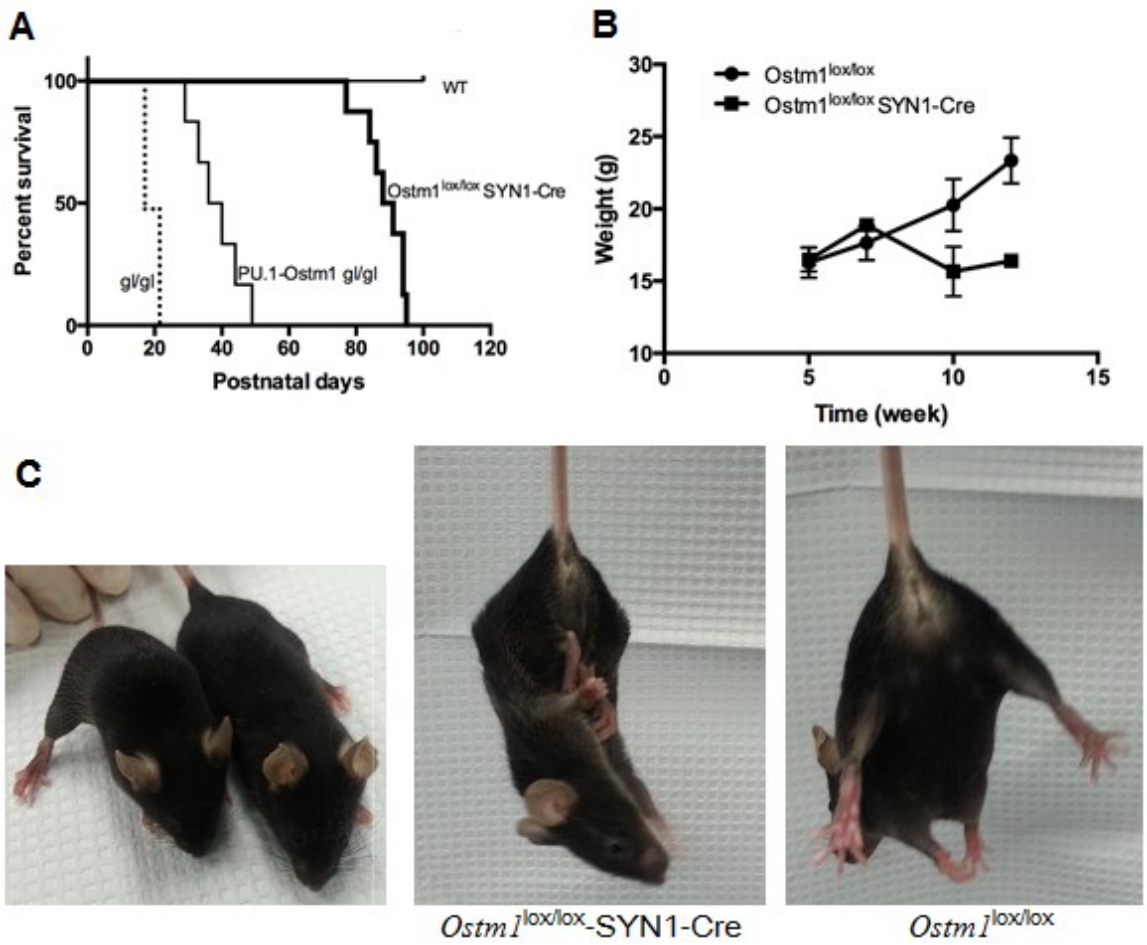

Figure 3-4: Survival and growth curve of *Ostm1*$^{lox/lox}$-SYN1-Cre and controls.
(A) Compared to *gl/gl* (3 weeks) and PU.1- *Ostm1-gl/gl*(6 weeks), *Ostm1*$^{lox/lox}$-SYN1-Cre mice had longer life span of 13 weeks. (B) The weight loss was evident from week 10 starting around week 8. (C) Phenotypic comparison of 13-week-old *Ostm1*$^{lox/lox}$-SYN1-Cre and *Ostm1*$^{lox/lox}$. The left picture shows that *Ostm1*$^{lox/lox}$-SYN1-Cre mouse was thinner and smaller with hunched back compared to the control. Abnormal limb-clasping analysis was noticeable in *Ostm1*$^{lox/lox}$-SYN1-Cre (middle) starting from week 8 compared to control littermate (right).

Since the mice showed abnormalities related to locomotion, we decided to analyze the mice with several behavioural tests.

3.4 Behavioural analysis of *Ostm1*$^{lox/lox}$-SYN1-Cre Mice

The phenotypic analysis led us to analyze locomotion and balance ability of the *Ostm1*$^{lox/lox}$-SYN1-Cre mice and the tests performed on these mice included the inverted grid test (to assess muscle strength), the 12mm and the 6mm balance beam tests (to assess motor balance), and the rotarod (to assess motor coordination and equilibrium) (Brooks and Dunnett 2009).

From all of these tests, the behaviour of recombinant mice at 4 weeks of age was undistinguishable compared to the other control groups. However by 8 weeks, the recombinant mice were greatly challenged by the tasks, although the results showed a tendency to improve performances by repeating tasks (Fig.3-5). By week 12, the recombinant mice have failed almost all the task that were tested (Fig.3-5).

Additionally, all of *Ostm1*$^{+/+}$-SYN1-Cre mice did not show any anomalies compared to *Ostm1*$^{+/+}$ mice. Therefore it can be concluded that SYN1-Cre alone has no effect on the phenotype. Also, *Ostm1*$^{lox/+}$SYN1-Cre with no phenotype demonstrated that loss of one allele has no effect. This is consistent with a recessive mutation as grey-lethal.

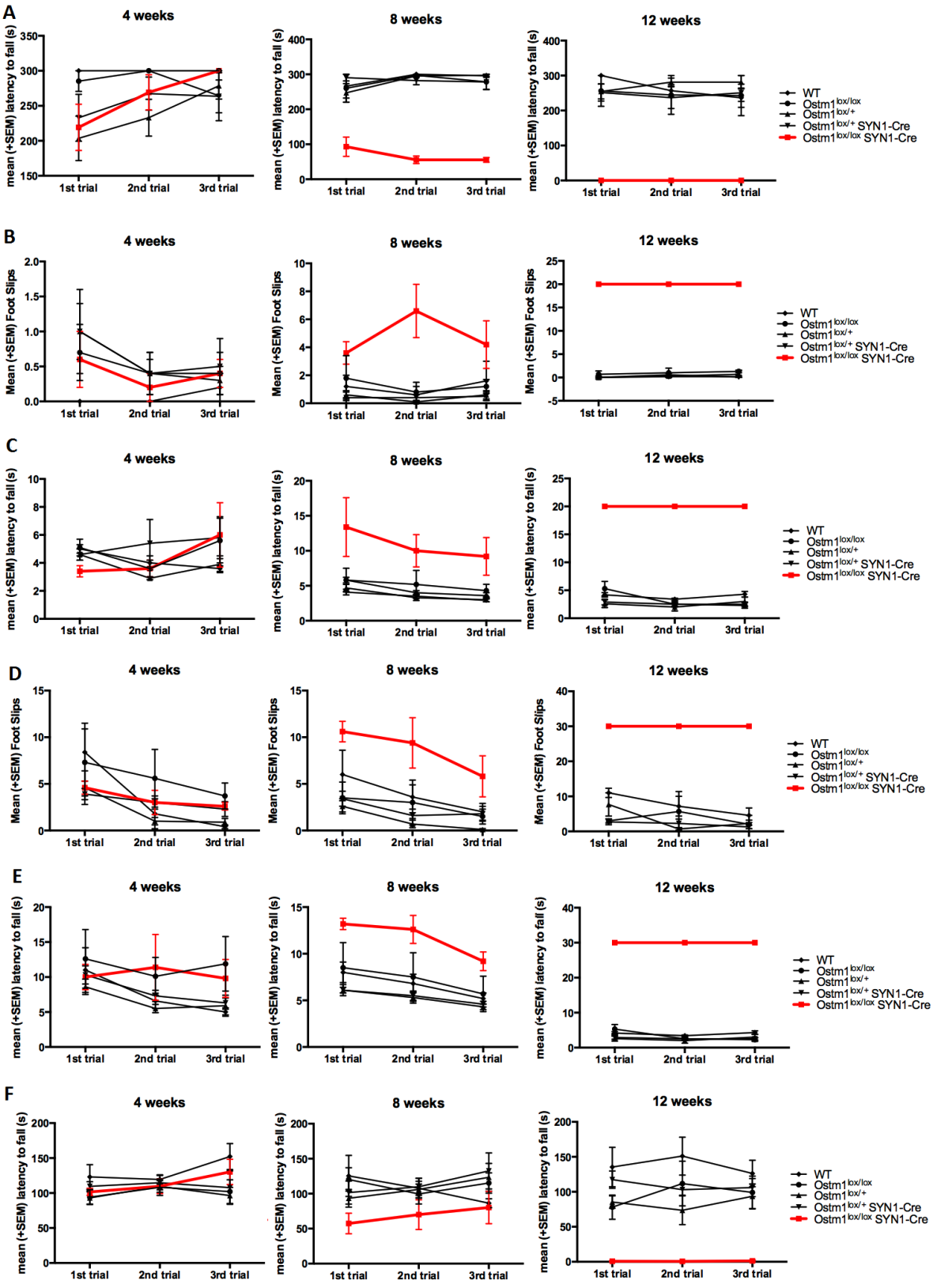
A
4 weeks
8 weeks
12 weeks
mean (+SEM) latency to fall (s)
1st trial
2nd trial
3rd trial
B
Mean (+SEM) Foot Slips
C
D
E
F
WT
Ostm1lox/lox
Ostm1lox/+
Ostm1lox/+ SYN1-Cre
Ostm1lox/lox SYN1-Cre

Figure 3-5: Analysis of locomotion and motor function of *Ostm1*$^{lox/lox}$-SYN1-Cre mice. The tests were done at week 4, at week 8, and at week 12. At each time point, the tests were repeated 3 times to show if the learning function is impaired. (A) Inverted grid test (B,C)12mm Balance Beam test (D,E) 6mm Balance Beam test (F) Rotarod (■ = *Ostm1*$^{lox/lox}$-SYN1-Cre (n=5) is highlighted in red, ◆ = wild-type (n=5), ●= *Ostm1*$^{lox/lox}$ (n=7), ▲= *Ostm1*$^{lox/+}$ (n=8), ▼= *Ostm1*$^{lox/+}$-SYN1-Cre (n=8))

The behaviour analysis showed that the *Ostm1*$^{lox/lox}$-SYN1-Cre mice developed a significant locomotion defect from week 8 even if it was not evident by simple *de visu* examination. The defect progressed rapidly to an extent that they failed the tasks at week 12.

Since the PU.1-*Ostm1-gl/gl* showed neurodegeneration and inflammatory response in the hippocampus, we hypothesized that the *Ostm1*$^{lox/lox}$-SYN1-Cre would have similar phenotype. The hippocampus is well known for its importance in learning and memory. So we expected to detect some learning and memory impairment together with locomotion defect. The mice, however, seemed to have normal learning ability at 8 weeks when they are still able to complete the task. Hence further analysis of learning and memory function was carried out using a novel object recognition test designed to examine the learning and memory (Antunes and Biala 2012). First, a mouse gets to explore two objects for 10 minutes before the objects are removed. After 2 hours, one of the objects is

changed with a new object (novel object). Mice with good learning and memory tend to spend more than 50% of time exploring the novel object.

The result for *Ostm1*$^{lox/lox}$-SYN1-Cre was controversial. The % of time spent for exploring novel object (% novel duration) of first 5 minutes was 66.38% which is the highest (Fig.3-6A) but the '% novel duration' decreased to 30.40% during the next 5 minutes which is the lowest compared to other controls(Fig.3-6B). Since impaired motor function of the mice may have an impact on the results, activity of the mice during these tests was recorded. Yet, there was no noticeable difference in the activity of the *Ostm1*$^{lox/lox}$-SYN1-Cre mice compared to other control mice (Fig.3-6C). Interestingly, the total duration of exploration was significantly decreased in the *Ostm1*$^{lox/lox}$-SYN1-Cre mice (Fig.2-6D). This suggests that the mice have some form of emotional impairment such as excess anxiety which make the interpretation of result, in terms of learning and memory, difficult.

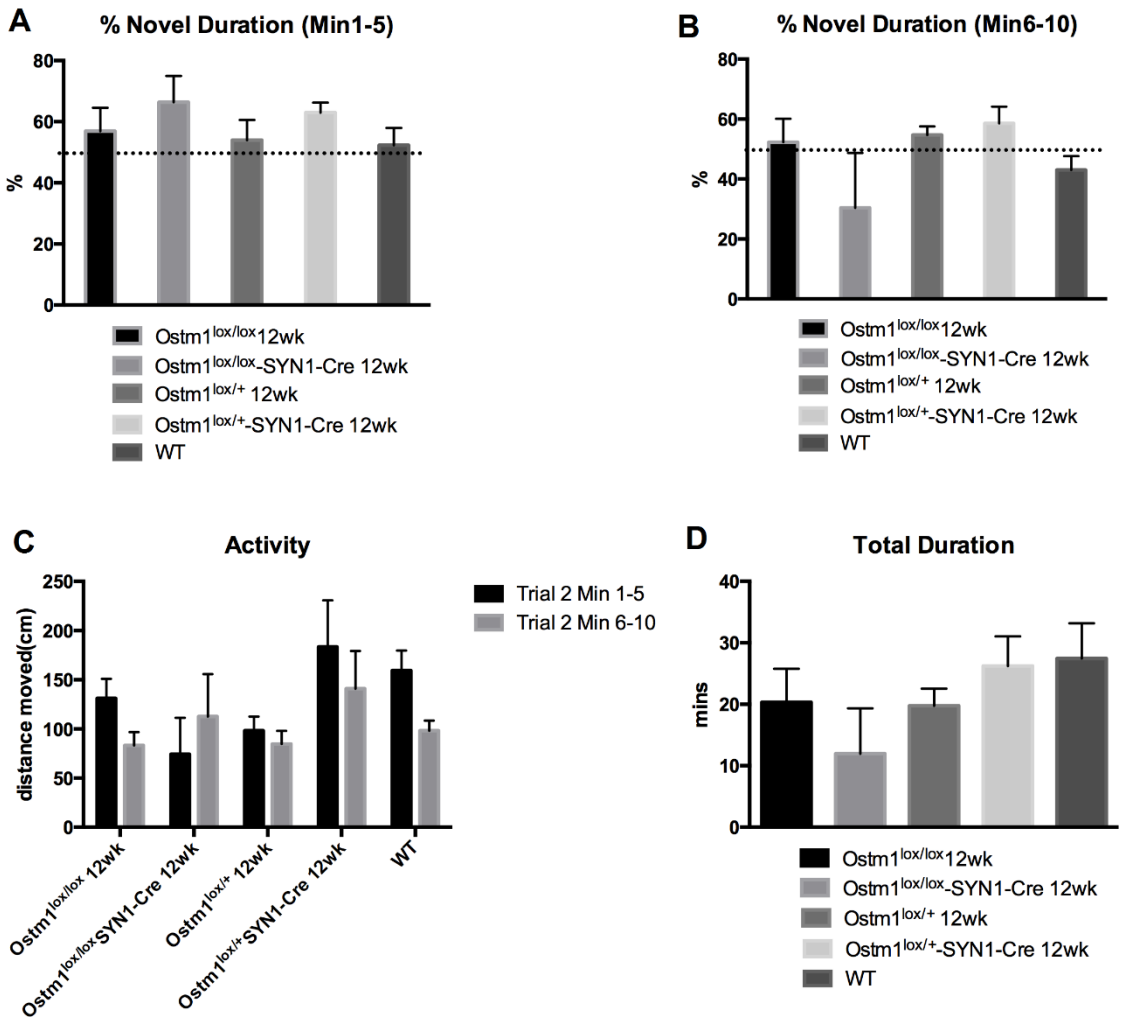

Figure 3-6: Analysis of learning and memory of *Ostm1*$^{lox/lox}$-SYN1-Cre mice. (A)Percentage time spent to explore the novel object for the first 5 minutes. (B)Percentage time spent to explore the novel object for the last 5 minutes. (C)Activity of mice demonstrated by the total distance moved during the test. (D)Total duration of time spent for exploring the both the familiar and the novel object. (*Ostm1*$^{lox/lox}$-SYN1-Cre: n=2, wild-type: n=10, *Ostm1*$^{lox/lox}$: n=6, *Ostm1*$^{lox/+}$: n=7, *Ostm1*$^{lox/+}$-SYN1-Cre: n=9)

The *Ostm1*$^{lox/lox}$-SYN1-Cre mice had locomotion and motor function impairment together with emotional impairment which needs to be examined further. These

analyses lead us to conclude that loss of Ostm1 function specifically in neuronal cells has a profound effect on the mouse behaviour. In order to establish a potential link between the brain specific defects and mouse behaviour, brain pathology of these mice was characterized.

3.5 Histological analysis of *Ostm1*$^{lox/lox}$-SYN1-Cre Mice

3.5.1 Hematoxylin and Eosin staining

From the H&E staining, the most evident difference between the *Ostm1*$^{lox/lox}$-SYN1-Cre and the control brain sections of 12-week-old mice is the loss of cornu ammonis 3 (CA3) and dentate gyrus (Hodgkinson, Moore et al.) of hippocampus.

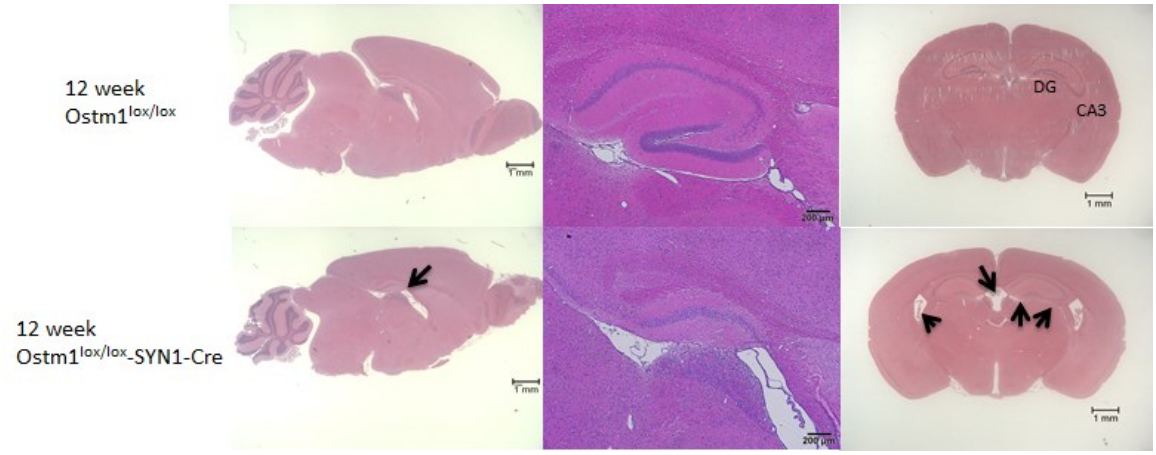

Figure 3-7: H&E staining of *Ostm1*$^{lox/lox}$-SYN1-Cre and control brain sections of 12-week-old mice. Loss of regions in hippocampus and enlarged ventricle is apparent in *Ostm1*$^{lox/lox}$-SYN1-Cre brain. Arrows indicate loss of CA3 and DG (left and right) and enlarged ventricles (right) in *Ostm1*$^{lox/lox}$-SYN1-Cre brain (Scale bar: left and right = 1mm, middle = 200µ)

These were similar observations but more severe compared to those of PU.1-*Ostm1-gl/gl* mice, a mouse model in which loss of CA3 region was observed.

Additionally, ventricles were enlarged in *Ostm1*$^{lox/lox}$-SYN1-Cre brain.
Since the PU.1 transgenic mice showed inflammation and neurodegeneration in the brain, the *Ostm1*$^{lox/lox}$-SYN1-Cre brain sections were analyzed with specific staining to visualize different cell types and compared to controls

3.5.2 Astrocytes activation in brain

Firstly, activated astrocytes were stained to examine inflammation in the brain. Since activated astrocytes express GFAP, GFAP staining was performed. At week 7, when the *Ostm1*$^{lox/lox}$-SYN1-Cre mice were phenotypically undistinguishable from the control mice, the astrocyte activation was slightly more pronounced in the cortex (Fig.3-8A) and in the hippocampus compared to control (Fig.3-8B). At week 12, the change was dramatic; the increase of activation in *Ostm1*$^{lox/lox}$-SYN1-Cre cortex was 4.6 fold and that in hippocampus was 3.5 fold compared to the control.

Interestingly, the increased astrocyte activation in cerebellum at *Ostm1*$^{lox/lox}$-SYN1-Cre brain was delayed and only observed from week 10 (Fig.3-8C).

Activation was observable in the granular layer, white matter and at dendrites of Purkinje cells.

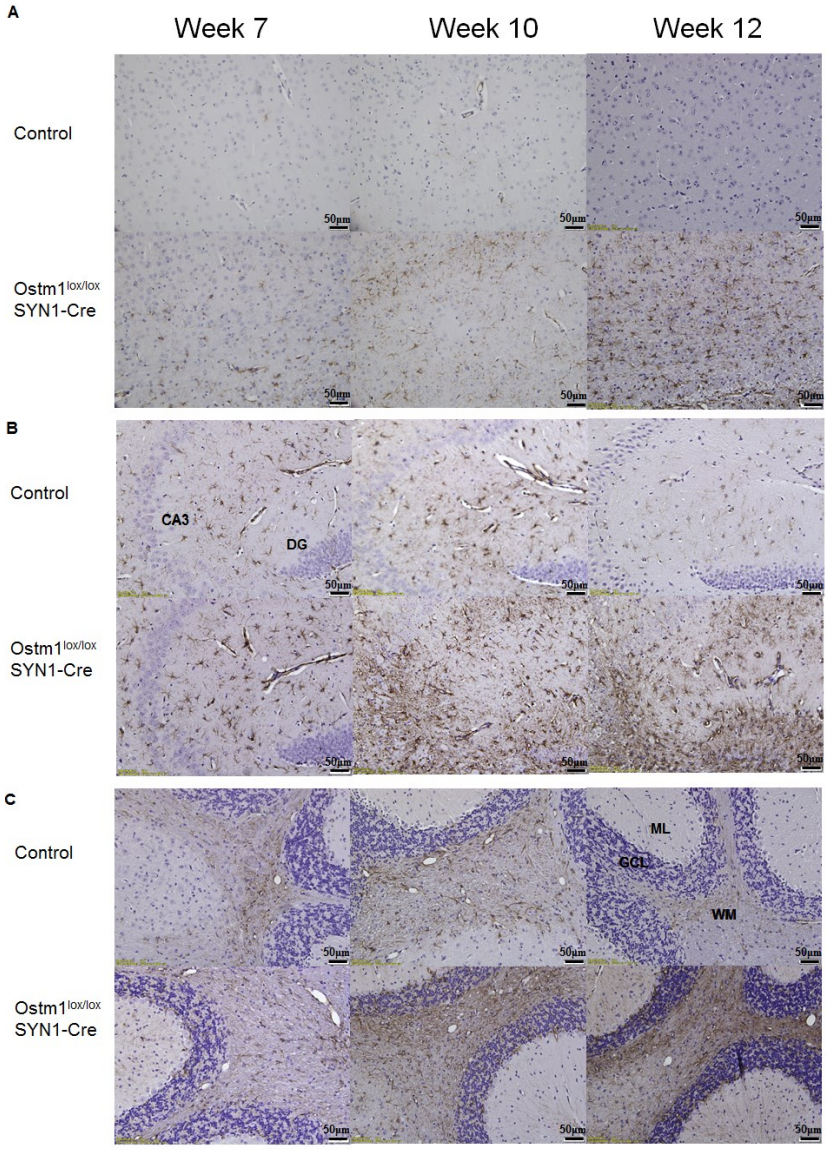

Figure 3-8: GFAP immunostaining of *Ostm1*$^{lox/lox}$-SYN1-Cre and control (*Ostm1*$^{lox/lox}$) brain sections. Immunostaining of cortex (A), hippocampus (B) and cerebellum (C) was done at 7, 10, and 12 weeks of age. (ML = Molecular Layer, GCL = Granular Cell Layer, WM = White Matter, scale bar = 50µm)

3.5.3 Neuronal degeneration in cortex and hippocampus

As the astrocyte activation was observable from week 7, neuronal populations were visualized with NeuN staining. Following the astrocyte activation detected from week 7, neurodegeneration was evident from week 10. The loss of cortical and hippocampal neurons was very clear (Fig.3-9). Especially in hippocampus, the loss of neurons in CA3 initiated at week 10 and by week 12, neurons in the CA3 and the DG were almost completely gone (Fig.3-9A). The cortical neurons were also degenerated from week 10 (Fig.3-9B).

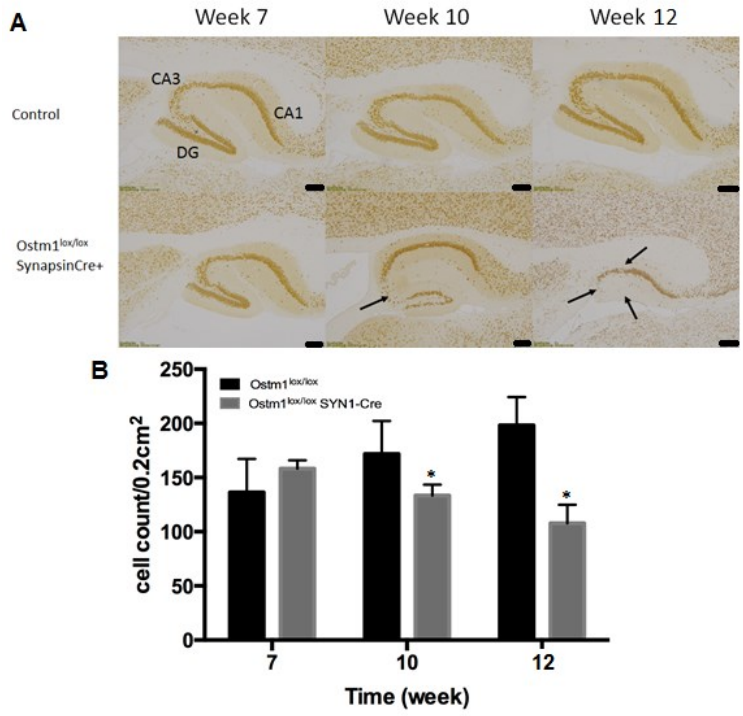

Figure 3-915: Progressive neurodegeneration in hippocampus of *Ostm1*$^{lox/lox}$-SYN1-Cre. (A) NeuN staining of hippocampus shows neuronal loss from week 10. Arrows indicating loss of CA3 at 10 weeks (middle) and loss of CA3 and DG at 12 weeks (right) (B) Cortex NeuN positive neuron counts were quantified at 5

regions of each section (0.2cm^2 sized). The number of NeuN positive cells decreased from week 10. (scale bar = 200μm, *: P<0.05)

Since the *Ostm1*$^{lox/lox}$-SYN1-Cre mice displayed locomotion defects and the cerebellum is involved in locomotion function, bran regions including Purkinje cells in mutant and control mice were characterized. Similarly to cortex and hippocampus, astrocyte activation (visualized by GFAP immunostaining) was also detected in white matter and the dendrites of Purkinje cells in cerebellum of *Ostm1*$^{lox/lox}$-SYN1-Cre compared to control as mentioned earlier (Fig.3-8C).

Surprisingly, the Calbindin immunostaining specific to Purkinje cells in cerebellum, does not detect major reduction in cell number in *Ostm1*$^{lox/lox}$ SYN1-Cre brain sections compared to control (Fig.3-10). Astrocyte activation in cerebellum was observed, though it was delayed compared to the other parts of the brain. Neurodegeneration may be in progress but Purkinje cell death was not detectable in *Ostm1*$^{lox/lox}$ SYN1-Cre mice at 12 week of age.

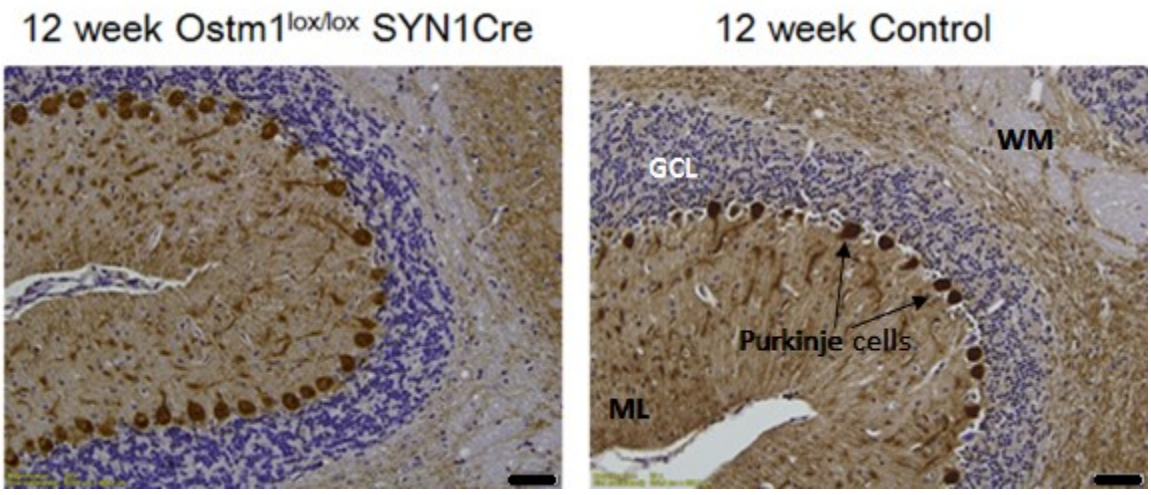

Figure 3-10: Calbindin immunostaining of *Ostm1*$^{lox/lox}$-SYN1-Cre cerebellum section. The nuclei of cells were stained with hematoxylin (Blue). *Ostm1*$^{lox/lox}$ was used as a control. (GCL=Granular Cell Layer, WM = White Matter, ML = Molecular Layer, scale bar = 50μm)

The histology analysis revealed widespread astrocyte activation in the brain specifically in hippocampus, in cortex and in cerebellum. The analysis also showed that the astrocyte activation occurs prior to the neurodegeneration in hippocampus and in cortex.

3.6 Molecular mechanisms associated with neurodegeneration in *Ostm1*$^{lox/lox}$-SYN1-Cre Mice

PU.1-*Ostm1-gl/gl* mice showed accumulation of autophagosomes(Héraud, Griffiths et al. 2014) which lead to degeneration in neuron, autophagy in the *Ostm1*$^{lox/lox}$-SYN1-Cre brain was examined.

3.6.1 Defective autophagy in brain

Autophagic pathway involves multiple steps. The very first step is the formation of autophagosomes. For the formation of autophagosome, autophagy related protein 7 (Atg7) activates Atg12 to conjugate with Atg5 (Yang, Liang et al. 2005). Then the Atg12-Atg5 conjugation recruits microtubule-associated protein 1 light chain 3 (LC3). The LC3 is found in 2 forms: LC3-I (Cytosolic form) and LC3-II (membrane bound form). The LC3-II is the credible marker of the autophagosome because it remains even after dissociation of Atg12-Atg5 (Yoshimori 2004). After the autophagosome formation, it undergoes maturation and fuses with lysosome to degrade the autophagic body (Yang, Liang et al. 2005).

To study autophagy in the brain, LC3-II/I ratio and level of ATG5 were determined. During the autophagosome formation, LC3-I is conjugated to phosphatidylethanolamine to form LC3-II and recruited to the membrane of autophagosomes (Tanida, Ueno et al. 2008). In the protein extracts of 12-week-old $Ostm1^{lox/lox}$-SYN1-Cre whole brain, the level of LC3-II was increased (Fig.3-11) indicating that there was autophagosome accumulation. Additionally, the level of ATG5 in 12-week-old $Ostm1^{lox/lox}$-SYN1-Cre whole brain was slightly

lowered compared to the control (Fig.3-11). Accumulation of autophagosomes may have some impact on the decreased level of ATG5.

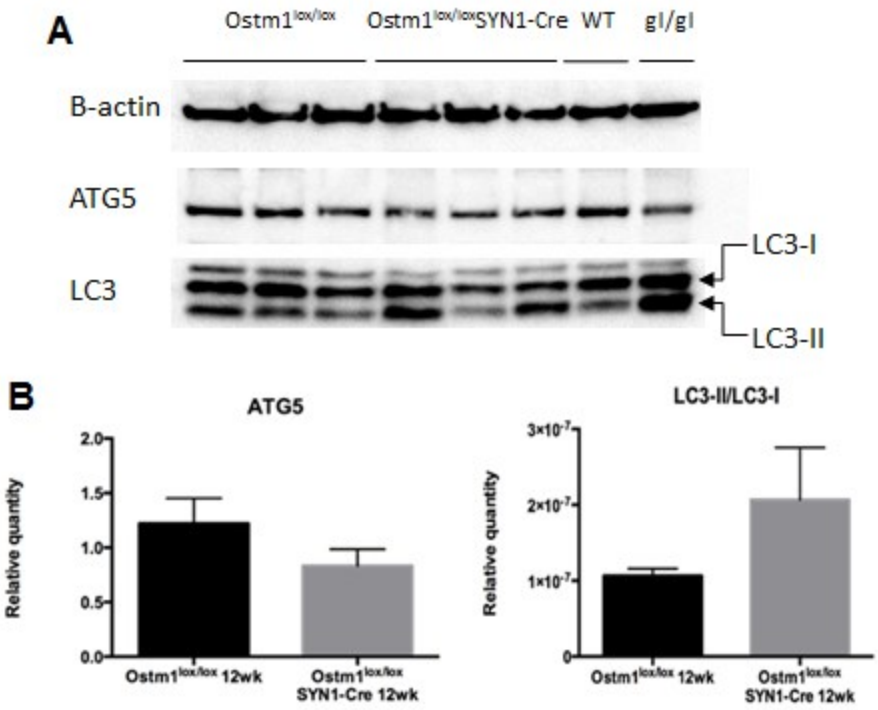

Figure 3-11: Abnormal autophagy in *Ostm1*$^{lox/lox}$-SYN1-Cre brain. (A) Western blot done with protein extract from whole brain of 12-week-old mice. (*Ostm1*$^{lox/lox}$ = 12-week-old *Ostm1*$^{lox/lox}$ mice, *Ostm1*$^{lox/lox}$-SYN1-Cre = 12-week-old, *Ostm1*$^{lox/lox}$-SYN1-Cre WT = 12-week-old wild-type mice. gl/gl = 3-week-old *gl/gl* mice, P-value=0.12) (B)Quantification of the level of proteins based on the western blot analysis. β-actin used as internal control (P-value=0.14)

3.7 Rescue of phenotypes in *Ostm1*$^{lox/lox}$-SYN1-Cre-SYN1-*Ostm1* mice

In order to definitively establish that the brain phenotypes were only due to the Osmt1 depletion in neuronal cells, bigenic *Ostm1*$^{lox/lox}$-SYN1-Cre-SYN1-*Ostm1* transgenic mice was generated (Fig.3-12) to test if the Ostm1 conditional knock-

out phenotype can be corrected with re-expression of the SYN1-*Ostm1* transgene.

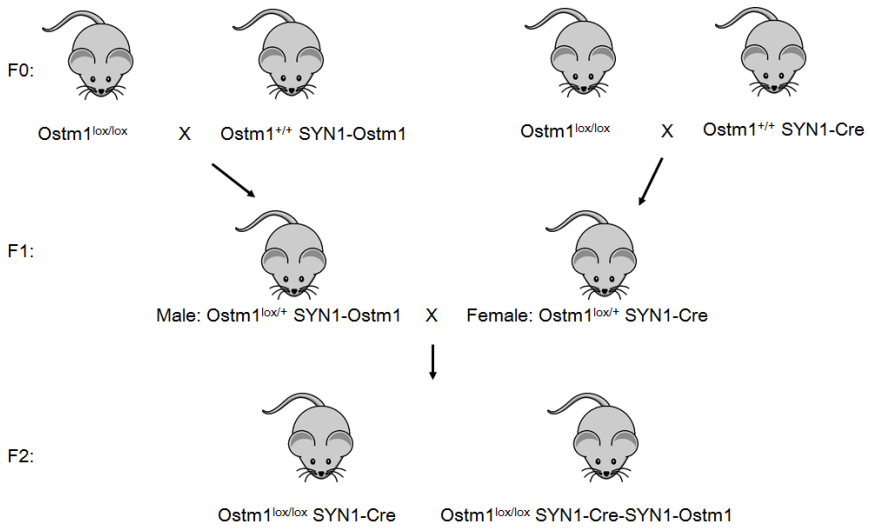

Figure 3-12: Mating scheme to generate *Ostm1*$^{lox/lox}$-SYN1-Cre-SYN1-*Ostm1* mice. To generate *Ostm1*$^{lox/lox}$-SYN1-Cre-SYN1-*Ostm1* mice, male *Ostm1*$^{lox/lox}$-SYN1-*Ostm1* mice (obtained from *Ostm1*$^{lox/lox}$ x *Ostm1*$^{+/+}$-SYN1-*Ostm1*)zz were crossed with *Ostm1*$^{lox/+}$-SYN1-Cre female mice (obtained from *Ostm1*$^{lox/lox}$ x *Ostm1*$^{+/+}$-SYN1-Cre).

Detailed brain histology of these bigenic mice was characterized by H&E staining and immunostaining with NeuN and GFAP compared to control. As shown in figure 3-13, bigenic brain sections showed a similar architecture compared to *Ostm1*^{loxlox} control with comparable hippocampus organization. In addition, astrocyte inflammation response in hippocampus, cortex and cerebellum was undetectable in bigenic mice compared to mutant samples. Together, these results strongly suggest that the neurodegenerative phenotype in Ostm1 mutant mice is only dependent of Ostm1 neuronal activity.

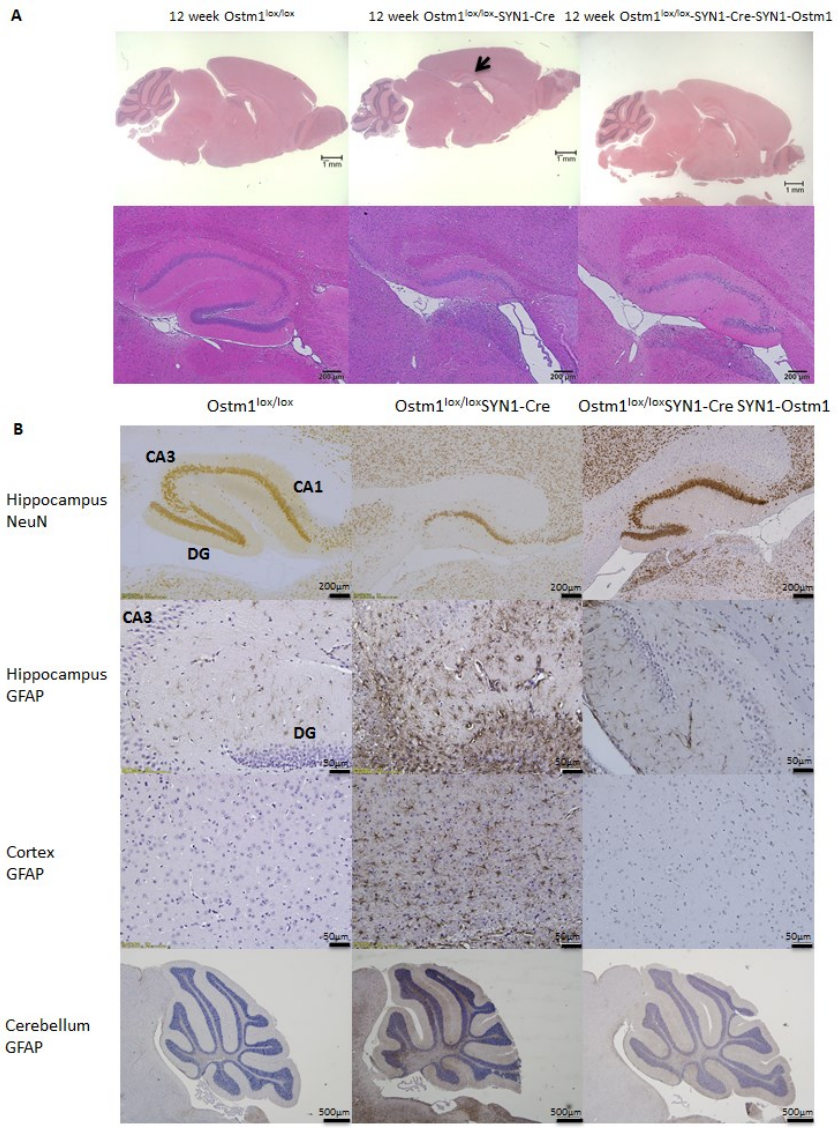

Figure 3-13: Rescue of phenotype in *Ostm1*$^{lox/lox}$-SYN1-Cre-SYN1-*Ostm1* brain section. (A)H&E staining on *Ostm1*$^{lox/lox}$-SYN1-Cre-SYN1-*Ostm1* brain. (Scale bar: top=1mm, bottom=200μm) (B)The *Ostm1*$^{lox/lox}$-SYN1-Cre-SYN1-*Ostm1* brain was stained with GFAP and with NeuN show the rescue of brain defect in *Ostm1*$^{lox/lox}$-SYN1-Cre. (scale bar: 1st row = 200μm, 2nd and 3rd row = 50μm, 4th row = 500μm)

Taken together, our results suggested a critical role of OSTM1 in neuronal homeostasis and physiology.

Chapter4. Discussion

Bone is a dynamic organ which constantly undergoes remodeling by osteoclasts and osteoblasts. Osteoclasts are cells that resorb the bone while osteoblasts are cells that is responsible for formation of the bone. Maintaining the balance of the functions of the two cell types is essential.

When the bone remodeling is impaired, one can suffer from skeletal disease. The most common disease is osteoporosis which is due to imbalance between bone formation and resorption. In contrast, failure in osteoclast function give rise to osteopetrosis. Osteopetrosis is a heterogeneous and heritable disorder which can be either caused by absence of osteoclasts, failure in osteoclast differentiation, or by non-functional osteoclasts.

Among many mutations resulting osteopetrosis, our lab is particularly interested in mutation in *OSTM1* gene which results in Autosomal Recessive Osteopetrosis. The *OSTM1*-related ARO patients have increased number of osteoclasts yet these cells are not functional as there is abnormal ruffled border formation. This results in ineffective osteoclasts with increase of bone marrow density (BMD) and bone marrow compartment is not properly formed which is characterized with

“bone in bone” appearance. Some patients display neurological defects in addition to hematopoietic defects.

In order to study the *OSTM1*-related ARO, we used grey-lethal *gl* mouse model which has a spontaneous null mutation in *Ostm1* gene and mirrors the osteopetrotic phenotype of *OSTM1* human patient. From the studies of the grey-lethal mouse model and of human cases, it was elucidated that *Ostm1* also has a primary role in different tissues, other than in bone. Especially, previous studies of PU.1-*Ostm1-gl/gl* mice and PU.1-*Ostm1*-SYN1-*Ostm1-gl/gl* mice showed that *Ostm1* has important role in the brain and particularly in neurons.

The purpose of the study presented in this thesis was to learn the role of *Ostm1* in neuronal physiology. For this purpose, Cre-lox system was used. The exon 5 of *Ostm1* was floxed then the floxed mice were crossed with SYN1-Cre deleter mice to induce specific ablation only in neurons.

Generation of conditional *Ostm1* knockout mice

For targeting knocking out OSTM1, rat synapsin I was chosen. The synapsin 1 is a well-known protein that regulates neurotransmitter release by interacting with synaptic vesicles (Greengard 1993, Hilfiker 1999, Hosaka, Hammer et al. 1999).

The SYN1-Cre mouse is known to abundantly express Cre recombinase in differentiated neurons from E12.5 and continue in the adult mouse (Zhu, Romero et al. 2001). One important factor to consider was that a low percentage of recombination was also found in testes and male SYN1-Cre progenies display germline recombination (Rempe, Vangeison et al. 2006). Thus only female SYN1-Cre mice were used in our crosses crosses and studies. The SYN1-Cre mice were crossed with loxed/loxed mice to finally produce *Ostm1*$^{lox/lox}$-SYN1-Cre.

The recombination efficiency in total brain tissue was ~27%. Knowing that SYN1-Cre expression is only in neurons (Zhu, Romero et al. 2001), the efficiency in neurons was estimated at ~77%. Since the *gl* mutation is recessive, it was important to have recombination efficiency more than 50%, 77% efficiency being in a range to mimic the recessive *gl* mutation. Moreover, the RNA expression level in neurons was 35% which is sufficient to result in a pathologic phenotype.

Compared to short life span of *gl/gl* mice (3 weeks) and of PU.1-*Ostm1-gl/gl* mice (6-8 weeks), *Ostm1*$^{lox/lox}$-SYN1-Cre mice have life span of ~13 weeks. Moreover, the notable difference, such as tremor, compared to control mice was observed only from 9 weeks. They showed significant weight loss from week 10 and the size of mouse was smaller and thinner with hunched back. As the mice aged,

they showed more balance problems as they often collapse while walking and abnormal limb-clasping response was observed. Together with the evidence of neurodegeneration of purkinje cells in cerebellum of PU.1-*Ostm1-gl/gl* (Héraud, Griffiths et al. 2014), it was suggested that locomotion and motor functions of the mice might be impaired due to *Ostm1* mutation in neurons.

The delay of phenotypes, compared to PU.1 *Ostm1-gl/gl*, may be because of 77% efficiency which causes lowering but not total absence of transcripts leading to some Ostm1 protein expression. Additionally, PU.1-*Ostm1-gl/gl* mice have *Ostm1* mutation in all tissues except those in cells of hematopoietic origin, which are corrected by PU.1. At the brain, the PU.1 transgenic mice had *Ostm1* mutation both in astrocytes and in neurons that can impact the severity and the timing of the phenotype. On top of everything, the timing of phenotype may be different because the background of the mice is different as *gl/gl* and PU.1-*Ostm1-gl/gl* is from the strain of GL/Le *d/J* +/+ *gl* whereas the *Ostm1*$^{lox/lox}$-SYN1-Cre is generated on C57BL/6.

Loss of *ostm1* in neurons results in locomotion and motor defects

Abnormal limb-clasping response of *Ostm1*$^{lox/lox}$-SYN1-Cre mice implies that neuronal loss and behavioural defect such as locomotion impairment occured.

The behaviour analysis examining locomotion of the mice confirmed that there is a progressive locomotion and motor defect in the *Ostm1*$^{lox/lox}$-SYN1-Cre mice starting from week 8. From all of the locomotion tests, the 4-week-old mice had no problem completing tasks as control groups. However at 8 weeks, the locomotion ability of *Ostm1*$^{lox/lox}$-SYN1-Cre mice was dramatically decreased and eventually the 12-week-old mice had failed all of the tasks. These results suggested that *Ostm1* mutation in neurons would affect more specifically the regions of brain that is responsible of locomotion function and/or the spinal cord.

The behaviour analysis and abnormal limb-clasping response, in fact, gives many possibilities of areas that may be affected by *Ostm1* mutation in neurons. First of all, defect in cerebellum is very common in mice and human with locomotion impairment. The *weaver* mutation of the *Girk2* is known for degeneration of cerebellar granular and Purkinje cells (Herrup and Trenkner 1987). Another common example of impairment in cerebellum is the *reeler* mutation affecting the *Reln* gene. They are characterized with disorganization of the cerebellum (Lblatt GJ 1998). Secondly, many mice mutants with locomotion impairments have anomalies in the basal ganglia especially in striatum. Huntington's Disease transgenic mice model shows neurodegeneration in striatum (Cheryl L. Wellington 2002, Bano D 2011). Degeneration in cerebral

cortex may be another cause of coordination deficit. Mice with *Atg7* knockout in CNS showed neurodegeneration in cerebral cortex and cerebellum (Komatsu, Waguri et al. 2006). Additionally, dopamine concentration may be affected. Dopamine is responsible of many physiological functions including control of coordinated movement and hormone secretion (Jackson and Westlind-Danielsson 1994). *Weaver* mice have reduced dopamine concentrations in dorsal striatum (Graybiel 1986, Triarhou LC 1988) and mice lacking dopamine D2 receptors showed locomotion impairment (Baik, Picetti et al. 1995). Lastly, motor neuron damage in spinal cord is a possible defect. In transgenic mice expressing the full-length mutated androgen receptor showed degeneration of α-motor neuron in spinal cord without changes in volume of cerebellum and striatum (McManamny, Chy et al. 2002). Based on these results, some of the possibilities to explain the *Ostm1*$^{lox/lox}$-SYN1-Cre phenotypes were analyzed in detail in this thesis, yet others may need to be further analyzed.

The locomotion tests allowed us to look at learning of the mice as well as the locomotion function. By repeating the locomotion test three times, we also examined the learning and memory function of the mice as well as for locomotion function. The 8-week-old *Ostm1*$^{lox/lox}$-SYN1-Cre mice, which can still complete the tasks, seemed to have normal learning ability compared to control. However,

knowing that there are many possibilities of affected area in CNS, we have performed a novel object recognition test to look at the learning and memory function of the mice.

Surprisingly, the object recognition result was controversial. The results showed that in the first five minutes of the novel exploration time, the mice have much better memory compared to control whereas the next five minutes, mice have far worse memory. Since there was a minimal decrease in total activity of *Ostm1*$^{lox/lox}$-SYN1-Cre mice, the controversy was not due to decreased activity. However, the total duration, time spent for exploring the familiar and the novel object, was significantly decreased. This suggests that the *Ostm1*$^{lox/lox}$-SYN1-Cre mice may have other kinds of emotional deficit, for example, excess anxiety or lowered reward value in exploring. Therefore, other behaviour tests such as the light-dark test or novelty suppression of feeding test should be done to explain these results.

Loss of *ostm1* in neurons leads to neurodegeneration and inflammation

The *Ostm1*$^{lox/lox}$-SYN1-Cre mice have longer lifespan and delayed behaviour phenotype compared to PU.1-*Ostm1-gl/gl* mice. Likewise, the histological analysis showed some delayed phenotypes. With the behaviour results and previous observation in PU.1-*Ostm1-gl/gl* mice, we focused on analyses in the cortex,

hippocampus and cerebellum. Importantly, there was no retinal degeneration detected in *Ostm1*$^{lox/lox}$-SYN1-Cre mice so the behaviour testing was possible.

From histological and immunohistochemical analysis, the neurodegeneration and astrocytes activation in these 3 regions was observed. *Ostm1*$^{lox/lox}$-SYN1-Cre mice have similar but delayed phenotypes compared to PU.1-*Ostm1-gl/gl* mice. Astrocyte activation was observed first from week 7 in hippocampus and cortex and from week 10 in cerebellum. Neuronal degeneration was also found. For hippocampus, CA3 neurons started to degenerate starting from week 10 then neuronal loss in DG to be defined appeared later. For cortex, the neuronal density decreased in all layers from week 10. In cerebellum, however, no neuronal degeneration was observed even at week 12.

It was surprising that there was no detectable neuronal degeneration in the cerebellum because it is the main part of the brain responsible for motor function and coordination. Yet, the severe astrocyte activation in cerebellum may be sufficient to affect the improper motor function. Moreover, the extensive astrocyte activation is the first sign of anomalies and eventually death in neurons. Investigation on early signs of degeneration may be helpful to analyze this. Additionally, the motor function is also controlled by other parts of the brain such

as cortex which have a severe neurodegeneration and inflammation response. We also looked at the spinal cord because the motor neurons in the spinal cord have great impact on the motor function. The spinal cord size (measured in coronal section) of *Ostm1*$^{lox/lox}$-SYN1-Cre at 12 week was decreased with severe neurodegeneration and enhanced inflammation. Although more analysis should be followed to investigate the impact in spinal cord, this preliminary data suggests that motor dysfunction may be due to neuronal loss in spinal cord.

Another interesting observation was the neurodegeneration in hippocampus. During the locomotion tests, *Ostm1*$^{lox/lox}$SYN1-Cre mice that are 8-week old seemed to have normal learning and memory ability as they improve as they repeat the tasks. However, 12-week-old mice were not able to complete any tasks so it was not possible to evaluate the memory functions. In 8- week-old mice, the anomalies in hippocampus were not severe enough yet to impair the learning and memory function.

In neurons, autophagy is an important mechanism of normal turnover of cytoplasmic contents. It has a protective role against neurodegeneration thus, impairment of autophagy leads to development of neurodegenerative disease (Jenny Fortun, William A. Dunn Jr et al. 2003, Ravikumar and Rubinsztein 2006, Sarkar, Ravikumar et al. 2009). Therefore insufficient autophagy, as these

Ostm1$^{lox/lox}$-SYN1-Cre mice, will cause neurodegeneration in hippocampus and cortex in the brain.

In fact, there was an increase of LC3-II/I level in the total brain extract from *Ostm1*$^{lox/lox}$-SYN1-Cre mice. This implied stimulation of autophagy with potential accumulation of autophagosomes (Kabeya, Mizushima et al. 2000). Since it seems to be a defect in autophagy, we looked at the Atg5 protein level, an earlier marker in autophagosome formation. Atg5 level was slightly decreased in the *Ostm1*$^{lox/lox}$-SYN1-Cre brain.

Interestingly, the *Atg5*$^{lox/lox}$-Nestin-Cre mice have neural cell specific deletion of *Atg5*. The Nestin-Cre expression was found from E10.5. At E15.5, when the Nestin-Cre has the peak expression, Atg5-dependent conversion of LC3-I to LC3-II was absent (Hara, Nakamura et al. 2006). Thus, there is a possibility of feedback between autophagosome formation and Atg5 level. Then decrease of Atg5 in *Ostm1*$^{lox/lox}$-SYN1-Cre brain may be due to the accumulation of autophagosomes. In turn, this will decrease the autophagosome formation and the entire autophagy process will slow down. Together with the abnormal metabolite accumulation in PU.1-*Ostm1-gl/gl* neurons(Héraud, Griffiths et al. 2014) and *Atg5*$^{lox/lox}$-Nestin-Cre neurons(Hara, Nakamura et al. 2006), the

Ostm1$^{lox/lox}$-SYN1-Cre brain may have accumulation of metabolites due to lowered autophagic pathway.

Rescue of defect in CNS by expression of *Ostm1* in neurons

In order to confirm the impact of *Ostm1* mutation in neuronal cells, we targeted *Ostm1* re-expression in neurons with the SYN1 promoter on the conditional ablation, *Ostm1*$^{lox/lox}$SYN1-Cre, background. SYN1-*Ostm1* mice were crossed with *Ostm1*$^{lox/lox}$SYN1-Cre to generate double transgenic *Ostm1*$^{lox/lox}$SYN1-Cre-SYN1-*Ostm1* mice.

The double transgenic mice were followed until 13 weeks and they did not show any behavioural anomalies with normal growth and no weight changes compared to wild-type mice. The life expectancy was also normal compare to control littermates. From the histological and immunohistological analysis, our study confirmed that there was a full phenotypic rescue. The brain of *Ostm1*$^{lox/lox}$SYN1-Cre-SYN1-*Ostm1* shows neither enhanced astrocyte activation nor neurodegeneration at 12 weeks of age compared to *Ostm1*$^{lox/lox}$SYN1-Cre mice. Therefore it can be concluded that the phenotypes observed in *Ostm1*$^{lox/lox}$SYN1-Cre mice were only due to loss of *Ostm1* in neuronal cells.

Conclusions and perspectives

A mutation in the OSTM1 gene has been solely implicated in the malfunctioning of osteoclasts, leading to osteopetrosis. Here we show that OSTM1 has significant functions in other tissues specifically in brain and neurons, using a mouse model of OSTM1-related ARO. (Héraud, Griffiths et al. 2014)

With regards to the Cre-lox system, *Ostm1*$^{lox/lox}$SYN1-Cre that have targeted knockout of *Ostm1* only in neurons was obtained. The *Ostm1*$^{lox/lox}$SYN1-Cre was generated to have recombination efficiency of ~77% and lowered the RNA expression to ~35%. This efficiency was in the range to mimic the recessive *gl* mutation. This model had lifespan of 13 weeks and showed behavioural anomaly of locomotion deficit from week 8.

Histological and immunohistochemical analysis allowed us to investigate the phenotypes in detail. The *Ostm1*$^{lox/lox}$-SYN1-Cre brain demonstrated neurodegeneration and inflammation in brain, especially in hippocampus, cortex, and cerebellum. The increased LCII/I ratio and lowered Atg5 level in total brain extract suggest that the anomalies found in brain may be due to accumulation of autophagosomes possibly with lowered autophagic pathway resulting in the difficulty of metabolite clearance in neurons.

Finally, by introducing the *Ostm1* expression back in neurons with SYN1 promoter, it was concluded that the phenotypes generated in *Ostm1*$^{lox/lox}$SYN1-Cre mice was only due to the absence of *Ostm1* in neurons. This is consistent with a monogenic and cell-autonomous neuronal defect.

There are many analyses to be done in the future. First of all, the novel object recognition test suggested that there may be a possibility of other emotional failure such as anxiety or lowered rewarding. This was also supported by the degeneration in hippocampus (Phelps 2004) as the hippocampus has important function regulating the emotional function as well as cortex (Maddock 1999). Behavioural test will be needed to evaluate the emotional deficit in *Ostm1*$^{lox/lox}$SYN1-Cre mice.

As the locomotion function is failing in the *Ostm1*$^{lox/lox}$SYN1-Cre mice, it is interesting to look at dopamine levels as well as motor neurons in spinal cord. Since several mice models with locomotion defect show the similar anomalies due to those factors (Graybiel 1986, Triarhou LC 1988, Jackson and Westlind-Danielsson 1994). Dopamine is known to control the hormone secretion (Jackson and Westlind-Danielsson 1994), such as norepinephrine, which may explain the

possible emotional impairment as well. Moreover, it will be worthwhile to look at anomalies in spinal cord and striatum, too.

It is very important to look at autophagy of the brain of *Ostm1*$^{lox/lox}$SYN1-Cre as it is a potential mechanism whose impairment that can lead to neuronal degeneration. It is necessary to focus on autophagy in neurons to confirm if there is the autophagosome accumulation, possibly by electronic microscopy and immunogold labelling. Another investigation to be done is to look at the mammalian target of rapamycin (mTOR) and protein kinase B (Akt) pathway which is largely involved in autophagy and neurodegenerative diseases (Heras-Sandoval, Pérez-Rojas et al. 2014). The activated mTOR and Akt were also lowered in PU.1-*Ostm1-gl/gl* brain (Héraud, Griffiths et al. 2014) and this further supports the need of investigating the mTOR and Akt pathways in neurons of the *Ostm1*$^{lox/lox}$-SYN1-Cre mice.

Lastly, it will be also very interesting to look at neuronal morphology of the *Ostm1*$^{lox/lox}$SYN1-Cre mice and grey-lethal mice possibly by primary neuron culture. This will allow us to further understand the role of *Ostm1* in neurons in the isolated environment.

From these studies and their analyses, we have gained a better understanding of cell autonomous role of *Ostm1* in neurons. Unfortunately, the results suggest that HSCT is not enough, even with the new approach of "in utero HSCT" (Sobacchi, Schulz et al. 2013), to completely treat *Ostm1* related ARO because of the role of OSTM1 neuron function. In 2009, it was shown that the human CNS stem cell transplantation to mice allowed the neuroprotection of host's CNS and the mice had delayed loss of motor coordination (Tamaki, Jacobs et al. 2009). Additionally in 2012, mice with severe demyelination were rescued with transplantation of human neural stem cell (Uchida, Chen et al. 2012). This approach may be a therapeutic avenue, together with HSCT, for *Ostm1*-related ARO human patients.

Apppendix 1

IRCM
Institut de recherches cliniques de Montréal

La formation et la recherche pour la vie

Comité de protection des animaux
Animal Care Committee

May 8th, 2013

Dr. Jean Vacher
Cellular Interactions and development

Subject: **Protocol 2013-07 entitled "Molecular analysis of osteopetrosis"**

Dear Colleague,

I'm pleased to inform you that the above mentioned protocol submitted to the Animal Care Committee has been formally approved. Please take note that this protocol is valid from May 8 2013 to March 31 2015.

I would like to remind you to label animal cages with the appropriate approved protocol number related to your project and to clearly indicate the protocol number in your purchase order of animals.

Best regards,

Dr. Javier Di Noia
Chair

110 avenue des Pins Ouest, Montréal (Québec) Canada H2W 1R7

http://intranet.ircm.qc.

Bibliography

Aker, M., A. Rouvinski, S. Hashavia, A. Ta-Shma, A. Shaag, S. Zenvirt, S. Israel, M. Weintraub, A. Taraboulos, Z. Bar-Shavit and O. Elpeleg (2012). "An SNX10 mutation causes malignant osteopetrosis of infancy." Journal of Medical Genetics **49**(4): 221-226.

Allen, N. J. and B. A. Barres (2009). "Neuroscience: Glia [mdash] more than just brain glue." Nature **457**(7230): 675-677.

Antunes, M. and G. Biala (2012). "The novel object recognition memory: neurobiology, test procedure, and its modifications." Cognitive Processing **13**(2): 93-110.

Baik, J.-H., R. Picetti, A. Saiardi, G. Thiriet, A. Dierich, A. Depaulis, M. Le Meur and E. Borrelli (1995). "Parkinsonian-like locomotor impairment in mice lacking dopamine D2 receptors." Nature **377**(6548): 424-428.

Bano D, Z. F., Mende Y, and Nicotera P (2011). "Neurodegenerative processes in Huntington's disease." Cell death and diesease **2**: e228.

Brenner, M. and A. Messing (1996). "GFAP Transgenic Mice." Methods **10**(3): 351-364.

Brooks, S. P. and S. B. Dunnett (2009). "Tests to assess motor phenotype in mice: a user's guide." Nat Rev Neurosci **10**(7): 519-529.

Chalhoub, N., N. Benachenhou, V. Rajapurohitam, M. Pata, M. Ferron, A. Frattini, A. Villa and J. Vacher (2003). "Grey-lethal mutation induces severe malignant autosomal recessive osteopetrosis in mouse and human." Nat Med **9**(4): 399-406.

Chen, Y., B. Wu, L. Xu, H. Li, J. Xia, W. Yin, Z. Li, D. Shi, S. Li, S. Lin, X. Shu and D. Pei (2012). "A SNX10/V-ATPase pathway regulates ciliogenesis in vitro and in vivo." Cell Res **22**(2): 333-345.

Cheryl L. Wellington, L. M. E., Claire-Anne Gutekunst, Danny Rogers, Simon Warby, Rona K. Graham, Odell Loubser, Jeremy van Raamsdonk, Roshni Singaraja, Yu-Zhou Yang, Juliette Gafni, Dale Bredesen, Steven M. Hersch, Blair R. Leavitt, Sophie Roy, Donald W. Nicholson, and Michael R. Hayden (2002). "Caspase Cleavage of Mutant Huntingtin Precedes Neurodegeneration in Huntington's Disease." The journal of Neuroscience **22**: 7862-7872.

Cleiren, E., O. Bénichou, E. Van Hul, J. Gram, J. Bollerslev, F. R. Singer, K. Beaverson, A. Aledo, M. P. Whyte, T. Yoneyama, M.-C. deVernejoul and W. Van Hul (2001). "Albers-Schönberg disease (autosomal dominant osteopetrosis, type II) results from mutations in the ClCN7 chloride channel gene." Human Molecular Genetics **10**(25): 2861-2867.

Coxon, F. P. and A. Taylor (2008). "Vesicular trafficking in osteoclasts." Seminars in Cell & Developmental Biology **19**(5): 424-433.

Del Fattore, A., A. Cappariello and A. Teti (2008). "Genetics, pathogenesis and complications of osteopetrosis." Bone **42**(1): 19-29.

Fdez, E. and S. Hilfiker (2006). "Vesicle pools and synapsins: New insights into old enigmas." Brain Cell Biology **35**(2-3): 107-115.

Graybiel, S. R.-T. a. A. M. (1986). "Expression of the weaver gene in dopamine-containing neural systems is dose-dependent and affects both striatal and nonstriatal regions." The journal of Neuroscience **6**: 3319-3330.

Greengard, P., Valtorta, F., Czernik, A. J., and Benfenati, F. (1993). "synaptic vesicle phosphoproteins and regulation of synaptic function." Science **259**: 780-785.

H, G. (1936). "Grey-lethal, a new mutation in the house mouse." J. heredity **27**: 105-109.

Hadjidakis, D. J. and I. I. Androulakis (2006). "Bone Remodeling." Annals of the New York Academy of Sciences **1092**(1): 385-396.

Hara, T., K. Nakamura, M. Matsui, A. Yamamoto, Y. Nakahara, R. Suzuki-Migishima, M. Yokoyama, K. Mishima, I. Saito, H. Okano and N. Mizushima (2006). "Suppression of basal autophagy in neural cells causes neurodegenerative disease in mice." Nature **441**(7095): 885-889.

HE, A.-S. (1904). "Röntgenbilder einer seltenen Knochenerkrankung." Munch Med Wochenschr **51**: 365–368.

Heras-Sandoval, D., J. M. Pérez-Rojas, J. Hernández-Damián and J. Pedraza-Chaverri (2014). "The role of PI3K/AKT/mTOR pathway in the modulation of autophagy and the clearance of protein aggregates in neurodegeneration." Cellular Signalling **26**(12): 2694-2701.

Héraud, C., A. Griffiths, S. N. M. Pandruvada, M. W. Kilimann, M. Pata and J. Vacher (2014). "Severe Neurodegeneration with Impaired Autophagy Mechanism Triggered by Ostm1 Deficiency." Journal of Biological Chemistry **289**(20): 13912-13925.

Herrup, K. and E. Trenkner (1987). "Regional differences in cytoarchitecture of the weaver cerebellum suggest a new model for weaver gene action." Neuroscience **23**(3): 871-885.

Hiesinger, P. R., A. Fayyazuddin, S. Q. Mehta, T. Rosenmund, K. L. Schulze, R. G. Zhai, P. Verstreken, Y. Cao, Y. Zhou, J. Kunz and H. J. Bellen (2005). "The v-ATPase V0 Subunit a1 Is Required for a Late Step in Synaptic Vesicle Exocytosis in Drosophila." Cell **121**(4): 607-620.

Hilfiker, S., Pieribone, V.A, Czernik, A.J., Kao, H.T, Augustine, G. J., and Greengard, P. (1999). "Synapsins as regulators of neurotransmitter release." Philos. Trans. R. Soc. Lond. B **354**: 269-279.

Hodgkinson, C. A., K. J. Moore, A. Nakayama, E. Steingrímsson, N. G. Copeland, N. A. Jenkins and H. Arnheiter (1993). "Mutations at the mouse microphthalmia locus are associated with defects in a gene encoding a novel basic-helix-loop-helix-zipper protein." Cell **74**(2): 395-404.

Hosaka, M., R. E. Hammer and T. C. Südhof (1999). "A Phospho-Switch Controls the Dynamic Association of Synapsins with Synaptic Vesicles." Neuron **24**(2): 377-387.

Jackson, D. M. and A. Westlind-Danielsson (1994). "Dopamine receptors: Molecular biology, biochemistry and behavioural aspects." Pharmacology & Therapeutics **64**(2): 291-370.

Jenny Fortun, William A. Dunn Jr, Shale Joy, a. Jie Li, L. Notterpek and Lucia Notterpek (2003). "emerging role for autophagy in the aggresomes in Schwann Cells." The journal of Neuroscience **23**(33): 10672-10680.

Kabeya, Y., N. Mizushima, T. Ueno, A. Yamamoto, T. Kirisako, T. Noda, E. Kominami, Y. Ohsumi and T. Yoshimori (2000). "LC3, a mammalian homologue of yeast Apg8p, is localized in autophagosome membranes after processing." The EMBO Journal **19**(21): 5720-5728

Kasper, D., R. Planells-Cases, J. C. Fuhrmann, O. Scheel, O. Zeitz, K. Ruether, A. Schmitt, M. Poët, R. Steinfeld, M. Schweizer, U. Kornak and T. J. Jentsch (2005). "Loss of the chloride channel ClC-7 leads to lysosomal storage disease and neurodegeneration." The EMBO Journal. **24**(5): 1079-1091

Komatsu, M., S. Waguri, T. Chiba, S. Murata, J.-i. Iwata, I. Tanida, T. Ueno, M. Koike, Y. Uchiyama, E. Kominami and K. Tanaka (2006). "Loss of autophagy in the central nervous system causes neurodegeneration in mice." Nature **441**(7095): 880-884.

Kong, Y.-Y., H. Yoshida, I. Sarosi, H.-L. Tan, E. Timms, C. Capparelli, S. Morony, A. J. Oliveira-dos-Santos, G. Van, A. Itie, W. Khoo, A. Wakeham, C. R. Dunstan, D. L. Lacey, T. W. Mak, W. J. Boyle and J. M. Penninger (1999). "OPGL is a key regulator of osteoclastogenesis, lymphocyte development and lymph-node organogenesis." Nature **397**(6717): 315-323.

Kornak, U., D. Kasper, M. R. Bösl, E. Kaiser, M. Schweizer, A. Schulz, W. Friedrich, G. Delling and T. J. Jentsch (2001). "Loss of the ClC-7 Chloride Channel Leads to Osteopetrosis in Mice and Man." Cell **104**(2): 205-215.

Lange, P. F., L. Wartosch, T. J. Jentsch and J. C. Fuhrmann (2006). "ClC-7 requires Ostm1 as a [beta]-subunit to support bone resorption and lysosomal function." Nature **440**(7081): 220-223.

Lblatt GJ, E. L. (1998). "Topographic and zonal organization of the olivocerebellar projection in the reeler mutant mouse." The Journal of Comparative Neurology **267**: 603-615.

Lee, Z. H. and H.-H. Kim (2003). "Signal transduction by receptor activator of nuclear factor kappa B in osteoclasts." Biochemical and Biophysical Research Communications **305**(2): 211-214.

Li, J., I. Sarosi, X.-Q. Yan, S. Morony, C. Capparelli, H.-L. Tan, S. McCabe, R. Elliott, S. Scully, G. Van, S. Kaufman, S.-C. Juan, Y. Sun, J. Tarpley, L. Martin, K. Christensen, J. McCabe, P. Kostenuik, H. Hsu, F. Fletcher, C. R. Dunstan, D. L. Lacey and W. J. Boyle (2000). "RANK is the intrinsic hematopoietic cell surface receptor that controls osteoclastogenesis and regulation of bone mass and calcium metabolism." Proceedings of the National Academy of Sciences **97**(4): 1566-1571.

Li, Y.-P., W. Chen, Y. Liang, E. Li and P. Stashenko (1999). "Atp6i-deficient mice exhibit severe osteopetrosis due to loss of osteoclast-mediated extracellular acidification." Nat Genet **23**(4): 447-451.

Maddock, R. J. (1999). "The retrosplenial cortex and emotion: new insights from functional neuroimaging of the human brain." Trends in Neurosciences **22**(7): 310-316.

Maranda, B., G. Chabot, J.-C. Décarie, M. Pata, B. Azeddine, A. Moreau and J. Vacher (2008). "Clinical and Cellular Manifestations of OSTM1-Related Infantile Osteopetrosis." Journal of Bone and Mineral Research **23**(2): 296-300.

McManamny, P., H. S. Chy, D. I. Finkelstein, R. G. Craythorn, P. J. Crack, I. Kola, S. S. Cheema, M. K. Horne, N. G. Wreford, M. K. O'Bryan, D. M. de Kretser and J. R. Morrison (2002). "A mouse model of spinal and bulbar muscular atrophy." Human Molecular Genetics **11**(18): 2103-2111.

Mégarbané, A., A. Pangrazio, A. Villa, E. Chouery, J. Maarawi, S. Sabbagh, G. Lefranc and C. Sobacchi (2013). "Homozygous stop mutation in the SNX10 gene in a consanguineous Iraqi boy with osteopetrosis and corpus callosum hypoplasia." European Journal of Medical Genetics **56**(1): 32-35.

Melloni, R. H. and L. J. Degennaro (1994). "Temporal onset of synapsin I gene expression coincides with neuronal differentiation during the development of the nervous system." The Journal of Comparative Neurology **342**(3): 449-462.

Nolte C, M. M., Pivneva T, Schipke CG, Ohlemeyer C, Hanisch UK, Kirchhoff F, Kettenmann H. (2001). "GFAP promoter-controlled EGFP-expressing transgenic mice: a tool to visualize astrocytes and astrogliosis in living brain tissue." Glia **33**(1): 72-86.

Ott, C.-E., B. Fischer, P. Schröter, R. Richter, N. Gupta, N. Verma, M. Kabra, S. Mundlos, A. Rajab, H. Neitzel and U. Kornak (2013) "Severe neuronopathic autosomal recessive osteopetrosis due to homozygous deletions affecting OSTM1." Bone **55**(2): 292-297.

Pangrazio, A., A. Fasth, A. Sbardellati, P. J. Orchard, K. A. Kasow, J. Raza, C. Albayrak, D. Albayrak, O. M. Vanakker, B. De Moerloose, A. Vellodi, L. D. Notarangelo, C. Schlack, G. Strauss, J.-S. Kühl, E. Caldana, N. Lo Iacono, L. Susani, U. Kornak, A. Schulz, P. Vezzoni, A. Villa and C. Sobacchi (2013). "SNX10 mutations define a subgroup of human autosomal recessive osteopetrosis with variable clinical severity." Journal of Bone and Mineral Research **28**(5): 1041-1049.

Pangrazio, A., P. L. Poliani, A. Megarbane, G. Lefranc, E. Lanino, M. Di Rocco, F. Rucci, F. Lucchini, M. Ravanini, F. Facchetti, M. Abinun, P. Vezzoni, A. Villa and A. Frattini (2006). "Mutations in OSTM1 (Grey Lethal) Define a Particularly Severe Form of Autosomal Recessive Osteopetrosis With Neural Involvement." Journal of Bone and Mineral Research **21**(7): 1098-1105.

Pata, M., C. Héraud and J. Vacher (2008). "OSTM1 Bone Defect Reveals an Intercellular Hematopoietic Crosstalk." Journal of Biological Chemistry **283**(45): 30522-30530.

Phelps, E. A. (2004). "Human emotion and memory: interactions of the amygdala and hippocampal complex." Current Opinion in Neurobiology **14**(2): 198-202.

Quarello, P., M. Forni, L. Barberis, C. Defilippi, M. F. Campagnoli, L. Silvestro, A. Frattini, N. Chalhoub, J. Vacher and U. Ramenghi (2004). "Severe Malignant Osteopetrosis Caused by a GL Gene Mutation." Journal of Bone and Mineral Research **19**(7): 1194-1199.

Rajapurohitam, V., N. Chalhoub, N. Benachenhou, L. Neff, R. Baron and J. Vacher (2001). "The mouse osteopetrotic grey-lethal mutation induces a defect in osteoclast maturation/function." Bone **28**(5): 513-523.

Ramírez, A., J. Faupel, I. Goebel, A. Stiller, S. Beyer, C. Stöckle, C. Hasan, U. Bode, U. Kornak and C. Kubisch (2004). "Identification of a novel mutation in the coding region of the grey-lethal gene OSTM1 in human malignant infantile osteopetrosis." Human Mutation **23**(5): 471-476.

Ravikumar, B. and D. C. Rubinsztein (2006). "Role of autophagy in the clearance of mutant huntingtin: A step towards therapy?" Molecular Aspects of Medicine **27**(5–6): 520-527.

Rempe, D., G. Vangeison, J. Hamilton, Y. Li, M. Jepson and H. J. Federoff (2006). "Synapsin I Cre transgene expression in male mice produces germline recombination in progeny." genesis **44**(1): 44-49.

Rodan, G. A. (1998). "Bone Homeostasis " PNAS **95**: 13361-13362.

Saftig, P., E. Hunziker, O. Wehmeyer, S. Jones, A. Boyde, W. Rommerskirch, J. D. Moritz, P. Schu and K. von Figura (1998). "Impaired osteoclastic bone resorption leads to osteopetrosis in cathepsin-K-deficient mice." Proceedings of the National Academy of Sciences **95**(23): 13453-13458.

Saito, M., P. I. Hanson and P. Schlesinger (2007). "Luminal Chloride-dependent Activation of Endosome Calcium Channels: PATCH CLAMP STUDY OF ENLARGED ENDOSOMES." Journal of Biological Chemistry **282**(37): 27327-27333.

Sarkar, S., B. Ravikumar and D. C. Rubinsztein (2009). Chapter 5 Autophagic Clearance of Aggregate-Prone Proteins Associated with Neurodegeneration. Methods in Enzymology. J. K. Daniel, Academic Press. **Volume 453:** 83-110.

Scimeca, J. C., A. Franchi, C. Trojani, H. Parrinello, J. Grosgeorge, C. Robert, O. Jaillon, C. Poirier, P. Gaudray and G. F. Carle (2000). "The gene encoding the mouse homologue of the human osteoclast-specific 116-kDa V-ATPase subunit bears a deletion in osteosclerotic (oc/oc) mutants." Bone **26**(3): 207-213.

SF, G. (2000). Osteogenesis: Development of Bones. Developmental Biology. Sunderland (MA), Sinauer Associates.

Sobacchi, C., A. Schulz, F. P. Coxon, A. Villa and M. H. Helfrich (2013). "Osteopetrosis: genetics, treatment and new insights into osteoclast function." Nat Rev Endocrinol **9**(9): 522-536.

Stauber, T. and T. J. Jentsch (2010). "Sorting Motifs of the Endosomal/Lysosomal CLC Chloride Transporters." Journal of Biological Chemistry **285**(45): 34537-34548.

Steward, C. G. (2003). "Neurological aspects of osteopetrosis." Neuropathology and Applied Neurobiology **29**(2): 87-97.

Sun-Wada, G.-H., T. Toyomura, Y. Murata, A. Yamamoto, M. Futai and Y. Wada (2006). "The a3 isoform of V-ATPase regulates insulin secretion from pancreatic β-cells." Journal of Cell Science **119**(21): 4531-4540.

Tamaki, S. J., Y. Jacobs, M. Dohse, A. Capela, J. D. Cooper, M. Reitsma, D. He, R. Tushinski, P. V. Belichenko, A. Salehi, W. Mobley, F. H. Gage, S. Huhn, A. S. Tsukamoto, I. L. Weissman and N. Uchida (2009). "Neuroprotection of Host Cells by Human Central Nervous System Stem Cells in a Mouse Model of Infantile Neuronal Ceroid Lipofuscinosis." Cell Stem Cell **5**(3): 310-319.

Tanida, I., T. Ueno and E. Kominami (2008). LC3 and Autophagy. Autophagosome and Phagosome. V. Deretic, Humana Press. **445:** 77-88.

Teitelbaum, S. L. (2000). "Bone Resorption by Osteoclasts." Science **289**(5484): 1504-1508.

Teitelbaum, S. L. and F. P. Ross (2003). "Genetic regulation of osteoclast development and function." Nat Rev Genet **4**(8): 638-649.

Tolar, J., S. L. Teitelbaum and P. J. Orchard (2004). "Osteopetrosis." New England Journal of Medicine **351**(27): 2839-2849.

Tondravi, M. M., S. R. McKercher, K. Anderson, J. M. Erdmann, M. Quiroz, R. Maki and S. L. Teitelbaum (1997). "Osteopetrosis in mice lacking haematopoietic transcription factor PU.1." Nature **386**(6620): 81-84.

Triarhou LC, N. J., Ghetti B (1988). "Mesencephalic dopamine cell deficit involves areas A8, A9 and A10 in weaver mutant mice." Experimental Brain research **70**: 256-265.

Uchida, N., K. Chen, M. Dohse, K. D. Hansen, J. Dean, J. R. Buser, A. Riddle, D. J. Beardsley, Y. Wan, X. Gong, T. Nguyen, B. J. Cummings, A. J. Anderson, S. J. Tamaki, A. Tsukamoto, I. L. Weissman, S. G. Matsumoto, L. S. Sherman, C. D. Kroenke and S. A. Back (2012). "Human Neural Stem Cells Induce Functional Myelination in Mice with Severe Dysmyelination." Science Translational Medicine **4**(155): 155ra136.

Wartosch, L., J. C. Fuhrmann, M. Schweizer, T. Stauber and T. J. Jentsch (2009). "Lysosomal degradation of endocytosed proteins depends on the chloride transport protein ClC-7." The FASEB Journal **23**(12): 4056-4068.

Wiktor-Jedrzejczak, W., A. Bartocci, A. W. Ferrante, A. Ahmed-Ansari, K. W. Sell, J. W. Pollard and E. R. Stanley (1990). "Total absence of colony-stimulating factor 1 in the macrophage-deficient osteopetrotic (op/op) mouse." Proceedings of the National Academy of Sciences **87**(12): 4828-4832.

Worby, C. A. and J. E. Dixon (2002). "Sorting out the cellular functions of sorting nexins." Nat Rev Mol Cell Biol **3**(12): 919-931.

Yang, Y.-p., Z.-q. Liang, Z.-l. Gu and Z.-h. Qin (2005). "Molecular mechanism and regulation of autophagy." Acta Pharmacol Sin **26**(12): 1421-1434.

Yoshimori, T. (2004). "Autophagy: a regulated bulk degradation process inside cells." Biochemical and Biophysical Research Communications **313**(2): 453-458.

Zhu, Y., M. I. Romero, P. Ghosh, Z. Ye, P. Charnay, E. J. Rushing, J. D. Marth and L. F. Parada (2001). "Ablation of NF1 function in neurons induces abnormal development of cerebral cortex and reactive gliosis in the brain." Genes & Development **15**(7): 859-876.